

Summer 2001

# Role of nitric oxide as a modulator of platelet dense granule release

Clifton Ford Frilot II

Follow this and additional works at: <https://digitalcommons.latech.edu/dissertations>

 Part of the [Biomedical Engineering and Bioengineering Commons](#)

---

## INFORMATION TO USERS

This manuscript has been reproduced from the microfilm master. UMI films the text directly from the original or copy submitted. Thus, some thesis and dissertation copies are in typewriter face, while others may be from any type of computer printer.

**The quality of this reproduction is dependent upon the quality of the copy submitted.** Broken or indistinct print, colored or poor quality illustrations and photographs, print bleedthrough, substandard margins, and improper alignment can adversely affect reproduction.

In the unlikely event that the author did not send UMI a complete manuscript and there are missing pages, these will be noted. Also, if unauthorized copyright material had to be removed, a note will indicate the deletion.

Oversize materials (e.g., maps, drawings, charts) are reproduced by sectioning the original, beginning at the upper left-hand corner and continuing from left to right in equal sections with small overlaps.

Photographs included in the original manuscript have been reproduced xerographically in this copy. Higher quality 6" x 9" black and white photographic prints are available for any photographs or illustrations appearing in this copy for an additional charge. Contact UMI directly to order.

ProQuest Information and Learning  
300 North Zeeb Road, Ann Arbor, MI 48106-1346 USA  
800-521-0600

UMI<sup>®</sup>



**ROLE OF NITRIC OXIDE AS A MODULATOR OF  
PLATELET DENSE GRANULE RELEASE**

**by**

**Clifton Ford Frilot II**

**A Dissertation Presented in Partial Fulfillment  
of the requirements for the Degree  
Doctor of Philosophy in Biomedical Engineering**

**COLLEGE OF ENGINEERING AND SCIENCE  
LOUISIANA TECH UNIVERSITY**

**August 2001**

UMI Number: 3017735

UMI<sup>®</sup>

---

UMI Microform 3017735

Copyright 2001 by Bell & Howell Information and Learning Company.

All rights reserved. This microform edition is protected against  
unauthorized copying under Title 17, United States Code.

---

Bell & Howell Information and Learning Company  
300 North Zeeb Road  
P.O. Box 1346  
Ann Arbor, MI 48106-1346

LOUISIANA TECH UNIVERSITY

THE GRADUATE SCHOOL

August 13, 2001

Date

We hereby recommend that the dissertation prepared under our supervision  
by Clifton Ford Frlot II

entitled Role of Nitric Oxide as a Modulator of Platelet Dense  
Granule Release

be accepted in partial fulfillment of the requirements for the Degree of  
Doctor of Philosophy in Biomedical Engineering

Steve Jones

Supervisor of Dissertation Research

Stan Napp

Head of Department

College of Engineering and Science

Department

Recommendation concurred in:

Stan Napp

Paul Hae, Jr.

Roy Henson

David Mills

Advisory Committee

Approved:

[Signature]

Director of Graduate Studies

Approved:

[Signature]

Director of the Graduate School

[Signature]

Dean of the College

## ABSTRACT

Nitric oxide (NO) has been shown to suppress platelet activation, induce vasodilation, inhibit smooth muscle cell proliferation, and act against infection. Activated platelets generally have opposite effects from these. They secrete platelet-derived growth factor (PDGF), which stimulates smooth muscle growth, serotonin, which is a platelet agonist, and a number of agents that promote further platelet aggregation. However, activated platelets also produce NO through the enzymatic functions of the constitutive form of nitric oxide synthase (NOS). The primary functions of this capability are not yet completely understood. Due to its low molecular weight and high diffusivity, NO is quickly transported from its source to surrounding tissues and medium, and this characteristic may be instrumental to its function. Understanding the way in which NO interacts with platelet function could assist in the development of improved diagnostic and surgical procedures as well as biomaterials that are resistant to thrombus formation. Due to the short half-life of NO *in vivo* and *in vitro*, it was desired to use platelet-derived serotonin and an indicator for NO function. The research objectives for this project were (1) to develop mathematical models representing the diffusive transport of platelet-derived agonists and inhibitors, (2) to electrochemically measure serotonin concentration during *in vitro* aggregation of platelets to fibrillar collagen with and without L-NMMA (a NO inhibitor), and (3) to verify platelet aggregation through histological analysis.

Presence of the NOS inhibitor, L-NMMA, did not have a statistical significance when compared across experiments with fibrillar collagen, which lacked L-NMMA. It can be inferred from this analysis that a statistically significant change in serotonin concentration, resulting from platelet activation by collagen, could not be detected when compared in presence and absence of the NOS inhibitor L-NMMA. From the research conducted in this project, many questions have been postulated concerning the primary role of NO in platelet function

## APPROVAL FOR SCHOLARLY DISSEMINATION

The author grants to the Prescott Memorial Library of Louisiana Tech University the right to reproduce, by appropriate methods, upon request, any or all portions of this Dissertation. It is understood that "proper request" consists of the agreement, on the part of the requesting party, that said reproduction is for his personal use and that subsequent reproduction will not occur without written approval of the author of this Dissertation. Further, any portions of the Dissertation used in books, papers, and other works must be appropriately referenced to this Dissertation.

Finally, the author of this Dissertation reserves the right to publish freely, in the literature, at any time, any or all portions of this Dissertation.

Author Clifton Ford Fulk II

Date 8/13/2001

## TABLE OF CONTENTS

ABSTRACT.....	iii
LIST OF TABLES.....	vii
LIST OF FIGURES.....	viii
ACKNOWLEDGMENTS.....	ix
CHAPTER 1 – INTRODUCTION.....	1
1.1 Background and Significance.....	1
1.1.1 Thrombosis Formation from Plaque Rupture.....	4
1.1.2 Limitations of Current Diagnosis.....	8
1.1.3 Coagulation Cascade.....	9
1.2 Platelets and Their Role in Hemostasis.....	12
1.3 Introduction to Voltammetry.....	24
1.3.1 Cyclic Voltammetry.....	25
1.3.2 Chronoamperometry.....	25
1.3.3 Differential Pulse Voltammetry.....	26
1.4 Hypothesis and Specific Aims.....	27
1.4.1 Hypothesis.....	28
1.4.2 Study Objectives.....	28
CHAPTER 2 – MATERIALS AND METHODS.....	30
2.1 Mathematical Models.....	30
2.1.1 Introduction to Mathematical Models.....	30
2.1.2 Model Assumptions.....	31
2.1.3 General Model Development.....	32
2.1.4 Solution to Agonist and Inhibitor Generation Model.....	34
2.1.5 Solution to Agonist Release Model.....	35
2.2 Preparation of Serotonin Sensor.....	36
2.2.1 Sensor Design and Fabrication.....	36
2.2.2 Supporting Instrumentation and Operation.....	39
2.3 Microelectrode Calibration and Analysis.....	41
2.3.1 Preparation of Phosphate Buffer.....	41
2.3.2 Electrochemical Pre-Treatment.....	42
2.3.3 Creation of Serotonin Standards.....	43
2.3.4 Calibration Protocol.....	44
2.3.5 Analysis of Sensor Data.....	45
2.4 Testing of Electrode in Blood.....	47

2.4.1 Blood Collection and Processing.....	47
2.4.2 Uric Acid Interference Study.....	48
2.4.3 Serotonin Calibration in Blood Variants.....	49
2.5 Static Study to Measure Serotonin Release from Platelets.....	49
2.5.1 Preparation of Platelet Suspensions.....	49
2.5.2 Preparation from Fibrillar Collagen Film.....	50
2.5.3 Serotonin Measurement in Dilute PRP.....	51
2.5.4 Histological Preparation and Analysis.....	52
2.5.5 Statistical Procedures.....	53
 CHAPTER 3 – RESULTS.....	 55
3.1 Mathematical Modeling.....	55
3.1.1 Agonist and Inhibitor Generation Model.....	55
3.1.2 Agonist Release Model.....	58
3.2 Serotonin Sensor Development.....	61
3.3 Sensor Calibration.....	63
3.3.1 Sensor Detection Limits.....	63
3.3.2 Power Law Regression of Calibration Data.....	64
3.4 Testing of Electrode in Blood.....	66
3.4.1 Uric Acid Interference.....	66
3.4.2 Testing in Blood Variants.....	67
3.5 Static Study to Measure Serotonin Release from Platelets.....	69
3.5.1 Evaluation of Fibrillar Collagen Film.....	69
3.5.2 Measurements in Dilute PRP.....	70
3.5.2.1 Single Factor ANOVA.....	71
3.5.2.2 Two-Factor ANOVA.....	73
3.5.3 Histological Analysis of Adhered Platelets.....	75
 CHAPTER 4 – DISCUSSION.....	 79
4.1 Mathematical Models.....	79
4.2 Experimental Evaluations.....	81
4.3 Serotonin Measurements and Data Analysis.....	84
4.4 Concluding Remarks.....	87
4.5 Recommendations for Future Research.....	89
 APPENDIX A – AGONIST AND INHIBITOR GENERATION MODEL.....	 92
 APPENDIX B – AGONIST RELEASE MODEL.....	 96
 LIST OF WORKS CITED.....	 100

## LIST OF TABLES

<b>Table Number</b>	<b>Title</b>	<b>Page Number</b>
1	Threshold values of platelet agonist .....	17
2	Species and inhibitors of interest for mathematical modeling.....	30
3	Creation of 5 mL serotonin standards for calibration .....	44
4	List of the four different experimental situations .....	49
5	Parameters for agonist and inhibitor generation model .....	55
6	Model parameters for agonist release model .....	59
7	Comparison between linear and power law correlation values .....	66
8	Possible interferences: the means and expected ranges of readily oxidizable, secretory products in adult human plasma.....	68
9	Serotonin data from static study in dilute PRP .....	71
10	ANOVA table for single factor experiment with four treatment levels .....	72
11	Two-factor ANOVA results (factors are experiment and trial).....	73
12	Data from platelet count of collagen surface for 40x and 100x (N = 5).....	77
13	Data from percent surface area coverage by platelets on collagen surface for 40x and 100x (N = 5) .....	78

## LIST OF FIGURES

Figure Number	Title	Page Number
1	Progression of atherosclerosis from the fatty streak to a clinical event (Adapted from Berliner <i>et al.</i> <sup>8</sup> ) .....	6
2	Coagulation cascade (Adapted from Turgeon <sup>15</sup> ) .....	9
3	Major divisions and contents of a typical platelet (From Turgeon <sup>15</sup> ) .....	13
4	Overall reaction for the enzymatic production of NO (Adapted from Knowles <i>et al.</i> <sup>36</sup> ) .....	21
5	Biological reactions of nitric oxide (Adapted from Beckman, <i>et al.</i> <sup>39</sup> ) .....	22
6	Working electrode potential in differential pulse voltammetry (Adapted from Skoog <i>et al.</i> <sup>43</sup> ) .....	26
7	Differential pulse voltammetry compared to cyclic voltammetry (Adapted from Princeton Applied Research, application note 155) .....	27
8	Physical parameters for mathematical model development.....	32
9	Species mass balance for differential shell with consumption .....	33
10	General fabrication process of serotonin sensor .....	38
11	Isolated Ag/AgCl reference electrode.....	40
12	Differential pulse voltammetry parameters for serotonin detection ..	41
13	Graphitic oxide surface structures found on carbon materials (from Kawagoe, <i>et al.</i> <sup>44</sup> ) .....	43

14	Electrochemical cell used for electrode calibration .....	45
15	Example of raw data analysis by Labview .....	47
16	Physical setup for serotonin measurement from dilute PRP .....	51
17	TxA2 transport .....	56
18	Thrombin transport .....	56
19	NO transport.....	57
20	Normalized steady-state concentration profiles of TxA2, thrombin, and NO .....	58
21	Serotonin transport.....	59
22	ADP transport .....	59
23	Carbon fiber tip of sensor made of two carbon fibers (100x).....	62
24	Sealed neck of sensor with protruding fiber (40x).....	62
25	Interface of carbon fibers with copper conductor (40x) .....	62
26	Deflections in DPV scan corresponding to 4 and 144 nM serotonin.....	63
27	Example of upper saturation limit from calibration.....	65
28	Example of power law for an electrode calibration .....	66
29	Fibrillar collagen coating in tissue culture dish (100x) .....	70
30	Interaction analysis for the two-factor ANOVA.....	74
31	A typical aggregate showing individual platelets with a 10 $\mu\text{m}$ scale (400x) .....	75
32	Adhered platelet aggregates on collagen (40x from experiment 2) .....	76
33	Adhered platelet aggregates on collagen (40x from experiment 4) .....	77
34	Platelet inhibition by PGI <sub>2</sub> .....	82

35	Model of PGI <sub>2</sub> and TxA <sub>2</sub> production and effects (From Gorman, 1979 <sup>62</sup> ) .....	83
36	<i>In vitro</i> flow simulation apparatus .....	90

## **ACKNOWLEDGEMENTS**

I am truly grateful for all those who have helped me complete this work. Without their help, I would never have been able to finish. I would first like to thank God for his presence and guidance in my endeavors throughout life. I thank my wife Sharon and my parents Clifton and Dorothy Frilot for their never-ending support in everything I have ever set out to do. It is their motivation and inspiration that allowed me to complete this major milestone in my life.

I would sincerely like to thank my mentor, Dr. Steven A. Jones, for his time and guidance throughout this project. Without his patience, dedication, and wonderful ideas, this project would have never been completed. I would also like to thank my committee for the help, guidance, and laboratory supplies.

I want also to thank Dr. Steven Patton for his willingness to answer questions, provision for laboratory equipment and supplies, and his instruction in electrochemistry. Without his assistance, this project would not have taken place. Further, I need to thank all the personnel at Louisiana Tech farm, especially Drs. Green and Murphy, who assisted me with blood collection for the project. Their cooperation and expertise is much appreciated.

# CHAPTER 1

## INTRODUCTION

### **1.1 Background and Significance**

Maintenance of homeostasis in human beings and other vertebrates is assisted by adequate perfusion of tissue with nutrient-rich blood. During certain pathologies, proper blood flow to critical tissue is reduced by stenoses or occlusions in the vasculature. Particularly, if the heart or brain is starved of blood for too long, a fatal myocardial infarction or stroke could result. The two main processes that contribute to occlusive arterial disease have been shown to be atherosclerosis and thrombus formation. Throughout life, atherosclerotic deposits infiltrate the initially healthy vasculature of the newborn focally, which by middle age affects many individuals with critical thromboses<sup>1</sup>. It has been estimated that 1.5 million myocardial infarctions occur annually in the United States, and at least 500,000 of those infarctions result in sudden death<sup>2</sup>.

Past researchers determined the pathogenesis of occlusive arterial disease is possibly due to one of two distinct mechanisms. One mechanism, championed by Virchow, suggests permeation of the endothelium and intima by lipid and associated molecules forms a lipid rich fibrous and smooth muscle plaque locally within the intima<sup>1</sup>. However, another hypothesis, developed by Rokitansky and furthered by Duguid, links the atherosclerotic process with thrombosis more closely in that development of

atherosclerosis is dependent on the presence of arterial thrombosis<sup>1</sup>. Thrombus formation is a multi-faceted process involving lipids, cytokines, leukocytes, cholesterol, coagulation proteins, cellular degradation products, and platelets.

Thrombus formation can occur at locations of atherosclerotic plaque rupture, damaged endothelium, or intact endothelium. Platelets are a major component of arterial thromboses, and they constantly survey the endothelial lining for discontinuities. When areas of vascular integrity are disrupted, platelets adhere to the exposed subendothelium and can recruit adjacent platelets to form a platelet plug over the site of vascular injury. Another function of platelets is initiation of tissue repair following injury. Platelets can secrete growth factors and mitogens in order to stimulate the growth of smooth muscle cells (SMCs) and other vascular components. Ideally, the platelet thrombus slowly dissolves away during the process of vessel repair, but during certain conditions it continues to grow. A growing thrombus can either proliferate until total occlusion results, or loose fragments of the aggregate can break off and cause an embolism in a smaller, distal vessel, thus causing a clinical event.

During certain flows, local hemodynamic forces can alter normal platelet function. Under conditions of low shear stress, platelets initially adhere to disrupted endothelium through interaction with the adhesive subendothelial proteins fibronectin, vitronectin, and von Willebrand factor (vWF). Adhesion of platelet membrane receptors to fibronectin is much faster than adhesion to vWF, but it is a reversible process that attenuates with increasing shear stress<sup>3</sup>. Elevated shear stress causes a conformation change in the integral platelet glycoprotein IIb-IIIa (GPIIb-IIIa), resulting in the exposure

of more vWF receptors. Due to vWF-mediated adhesion, platelet adhesion to damaged endothelium also occurs at locations of high shear stresses.

With the increased local velocities found at a stenosis, areas of high shear stress, recirculation, and turbulence can occur resulting in enhanced transport of platelets and their contents to the vessel lumen. In these areas of recirculation, platelets have a longer residence time, causing an increased concentration of resting and activated platelets. Increases in shear stress cause erythrocytes to congregate towards the center of the flow, thus forcing platelets towards the periphery. This development results in an enhanced diffusion of platelets and their contents to the vessel wall. Conditions such as these can result in platelet adhesion and activation at locations of intact endothelium. Atherosclerosis formation with subsequent plaque rupture is similar to this situation.

Platelets and endothelial cells (ECs) have been shown to manufacture and secrete endothelium-derived relaxation factor (EDRF), a molecule that causes vessel vasodilation and inhibits platelet activation and aggregation. In the past few years, EDRF had been deduced to be nitric oxide (NO). With regard to the platelet, NO has the opposite function of the other constituents the platelet possesses. Although NO has been shown to inhibit mitogenesis, act against infection, promote vasodilation, and inhibit coagulation, researchers still do not know if the platelet alone can produce the threshold concentrations required for these physiological actions. Due to the local amplification of coagulation factors, platelet deposition, and fibrinogen polymerization to fibrin, the coagulation cascade is referred to as a positive feedback mechanism. However, platelet inhibition and the subsequent attenuation of the coagulation cascade may be regulated or modulated by local concentrations of NO. Thus, the interaction between NO and platelet

activators, such as adenosine diphosphate (ADP), thromboxane A<sub>2</sub> (TxA<sub>2</sub>), and serotonin, may represent a negative feedback mechanism for platelet activation and thrombus formation. The positive and negative feedback mechanisms may become dominant under different circumstances that depend on local concentrations of agonists and hence on the diffusion process. Although NO is generated by platelets, its primary role with respect to the platelet is still unclear.

In the past, it has been suggested that a fundamental role of the platelet within the mammalian circulation is host defense against invasion by foreign organisms<sup>4</sup>. In some lower organisms, such as caterpillars, foreign-body responses are initiated by the adhesion of hemocytes (primitive leukocytes) to the foreign-body surface, with subsequent increased aggregation of neighboring hemocytes<sup>5</sup>. The end result is similar to a hemostatic platelet plug in mammals. This discovery suggests that primary hemostasis in higher mammals might be a phylogenetic vestige kept from the behavior of hemocytes<sup>6</sup>.

### **1.1.1 Thrombosis Formation from Plaque Rupture**

The fatty streak is the first noticeable lesion in atherosclerosis formation. In lesion-prone areas, increased endothelial cell (EC) permeability and activation result in the transport of plasma macromolecules into the intima<sup>7</sup>. With this flux of macromolecules, low-density lipoprotein (LDL) is trapped within the intima and subsequent oxidative modification of LDL occurs. Oxidized LDL is then recognized by the scavenger receptor and endocytosed by monocyte-derived macrophages, which contribute their enormous oxidative capacity<sup>8</sup>. With macrophages present, LDL lipids are oxidized further, but modification of the protein portion of LDL leads to loss of

recognition by the scavenger receptor. Changes in receptor recognition result in macrophage uptake of LDL by receptors unregulated by the cell's cholesterol content <sup>8</sup>. This process contributes to foam cell formation, the hallmark of the arterial fatty streak.

Following fatty streak formation, intimal SMCs proliferate and secrete abundant collagen rich matrix, forming an elevated intimal lesion termed the mature atherosclerotic plaque <sup>7</sup>. Mature plaque contains a core of a soft atheromatous material and hard SMC-related sclerotic tissue. The core is separated from the vascular lumen by a fibrous cap mainly composed of collagen, SMCs, and inflamed macrophages. Contents of the atheromatous material, commonly called gruel, include crystalline cholesterol, cholesterol esters, phospholipids, cellular degradation products, and collagen remnants <sup>9</sup>. During the process of atherogenesis, the endothelium is usually intact, but denuded areas, related to foam cell infiltration of the atherosclerotic plaque, also exist. Advanced plaques causing severe stenoses have a higher fibrous and lower atheromatous content (less than 20%) than those producing less severe lesions <sup>7,10</sup>. By itself, atherosclerosis does not induce clinical events, but plaque rupture or dislodgement can trigger a cascade of events, possibly culminating to a stroke or myocardial infarction. Figure 1 illustrates the sequence of events from the fatty streak to a clinical event.

Since arterial plaques are constantly subjected to mechanical stresses, they are prone to rupture, and the occurrence of plaque rupture is unpredictable. Thinning of the fibrous cap, located above the atheromatous core, probably precedes plaque rupture. The thinnest portion of the fibrous cap is densely populated with macrophages, and is located at the junction of the cap with the vessel lumen. Tears, leading to plaque rupture, commonly develop at this location. Macrophages are capable of destroying extracellular

matrix by phagocytosis or by secreting proteolytic enzymes, such as plasminogen activators and metalloproteinases, which weakens the fibrous cap, predisposing it to rupture <sup>7</sup>.

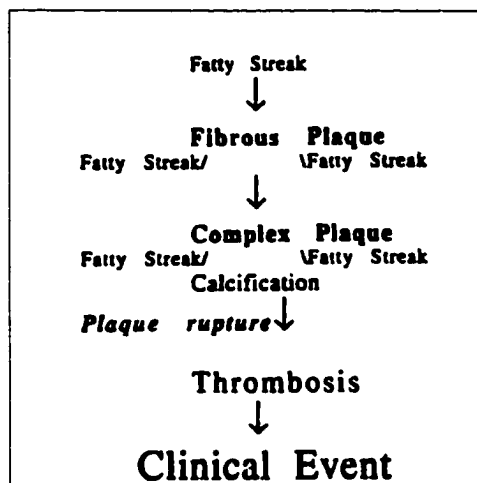


**Figure 1 - Progression of atherosclerosis from the fatty streak to a clinical event  
(Adapted from Berliner, et al <sup>8</sup>)**

Intrinsic properties of the fibrous cap determine the vulnerability to rupture, but external factors expedite the process.

When arterial plaques form a stenosis, velocity gradients within the narrowing vessel increase, thus creating regions of elevated shear stress. At locations proximal and distal to the stenosis, areas of turbulence, recirculation, and non-uniform flow can possibly develop. Zones of recirculation result in longer platelet residence times and an increase in the transport of platelets to the vessel wall results. Increased presence of activated platelets at the vessel wall can advance the progression of atherosclerosis through the secretion of platelet-derived growth factors and activation of neighboring platelets. If these conditions persist, a platelet-rich thrombus can begin to grow. Through vWF-mediated adhesion, platelets can adhere to the sub-endothelium of

ruptured atherosclerotic vessels, despite the presence high shear stresses. Elevated levels of shear stress enhance vWF-mediated adhesion <sup>3,11</sup>.

Factors such as shear stress due to a stenosis, sudden pressure changes, external compression, bending of eccentric plaques at their edges as a result of the propagating pulse wave, or changes in vasomotor tone could tear the thin fibrous cap. Coronary artery lesions appear to be more susceptible to rupture due to the bending and twisting of the artery during each heart contraction, and they are also exposed to two major changes in flow velocity during systole, compared with a single oscillation for other major visceral arteries <sup>12,13</sup>. Hard sclerotic plaques with a high SMC and collagen content are fairly resistant to stress, while soft atheromatous plaques with an expanding core of extracellular lipid and a thin fibrous cap are unstable and vulnerable <sup>9</sup>. Upon plaque rupture, lipid-rich atheromatous gruel, which is highly thrombogenic, is exposed to flowing blood. Atheromatous gruel is six-fold more thrombogenic than the collagen-rich sclerotic component of the lesion <sup>7</sup>. With a highly thrombogenic surface exposed, thrombotic response to plaque rupture follows. Three major factors that determine the thrombotic response to plaque rupture are (1) character and extent of exposed thrombogenic substrates (2) degree of stenosis and surface irregularities and (3) thrombotic-thrombolytic equilibrium at the time of plaque disruption <sup>9</sup>. Plaque growth is an unpredictable event explained by the occurrence of plaque rupture with subsequent hemorrhage into the plaque and/or mural thrombosis resulting in a stepwise plaque growth <sup>7</sup>. Most disrupted plaques are resealed by a small mural thrombus, and only sometimes does a major occlusive thrombus form <sup>14</sup>. Advanced knowledge on the

mechanism of thrombus formation and the inhibitory role of NO would help to develop procedures to better treat and diagnose critical thrombus formations at an earlier stage.

### **1.1.2 Limitations of Current Diagnosis**

Currently, angiography is the best imaging technique physicians use to quantify the degree of coronary arterial stenosis. Although angiography provides good evaluation of coronary circulation, it has some critical limitations. Sections of the coronary artery that appear normal on the angiogram are used as a reference for the assessment of stenotic lesions, but atherosclerosis is a diffuse process that involves vessel segments that appear geometrically normal. For example, it has been shown that coronary arteries enlarge in relation to the presence of atherosclerosis, and the luminal cross-sectional area may be preserved despite the presence of vessel disease<sup>12</sup>. Thus, physicians can act only on vessels that appear stenosed or occluded on the angiogram. A vessel lesion, which reduces the arterial diameter by 50%, is considered borderline severity, but it can have an atheromatous mass capable of decreasing the arterial cross sectional area by 75%<sup>12</sup>. Giroud *et al.* found that 78% of segments responsible for myocardial infarction were less than 50% stenosed on a previous angiogram, and Ambrose *et al.* showed the average degree of lesion stenosis resulting in myocardial infarction is 48%<sup>10</sup>. It has also been shown in two-thirds of patients with an acute ischemic syndrome that the responsible lesion was diagnosed insignificant on a previous angiogram<sup>10</sup>. Angiography is a useful tool for the local severity of coronary lesions but is limited as a predictor of future coronary occlusions. Since coronary artery disease follows a nonlinear course, plaque rupture and location of future occlusions are highly unpredictable events<sup>7,12</sup>.

### 1.1.3 Coagulation Cascade

The coagulation cascade is sub-divided into two different pathways, the extrinsic and intrinsic. Platelets are essential for proper function of the coagulation cascade. Both the intrinsic and extrinsic systems share specific coagulation factors with the common pathway. Figure 2 illustrates the cascade theory of blood coagulation for hemostasis.

The common pathway begins with the conversion of coagulation factor X to Xa and ends with fibrin formation. Secondary hemostasis is the term used to designate the coagulation factors' role in the hemostatic mechanism.

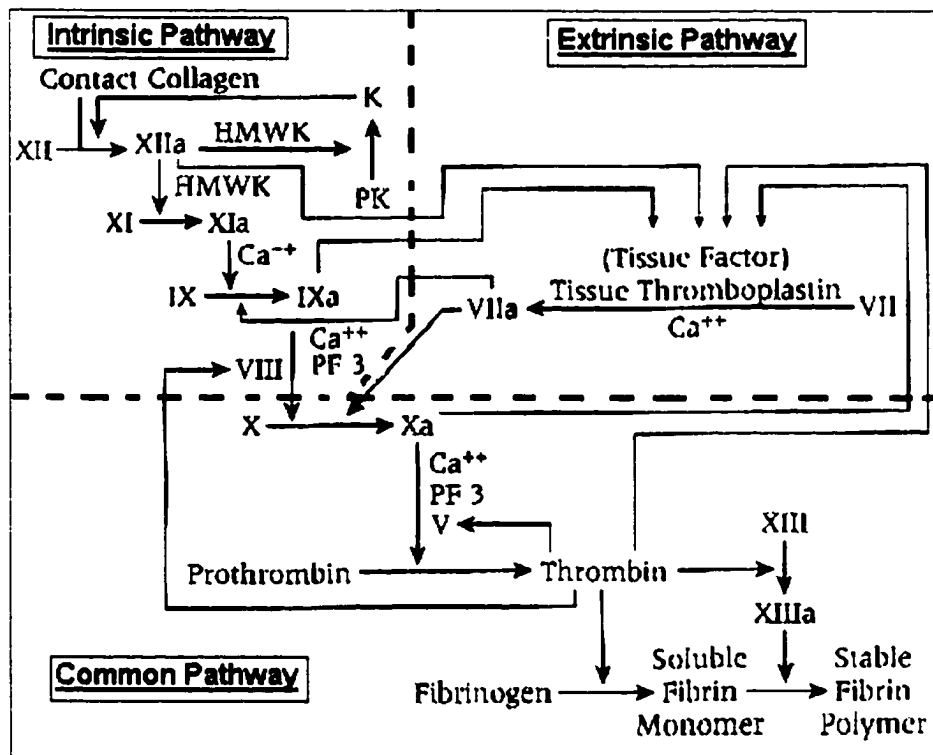


Figure 2 - Coagulation cascade (Adapted from Turgeon 15)

According to the cascade theory, each coagulation factor is converted to its active form by the preceding factor in a series of biochemical chain reactions<sup>16</sup>. Initiation of coagulation can occur by either the intrinsic or extrinsic pathway, but both pathways

converge with the common pathway, which converts soluble fibrinogen into an insoluble-gelatinous fibrin clot. As factor Xa enters the common pathway, factor V, ionic calcium ( $\text{Ca}^{2+}$ ), and platelet factor 3 (PF3) convert prothrombin (factor II) into thrombin, which is the active form of factor II. Association of factor Xa, factor V, PF3, and  $\text{Ca}^{2+}$  on the platelet membrane surface is called the prothrombinase complex. Activated platelets support binding of the IXa/VIIIa and Xa/Va complexes, which functions to localize and induce coagulant activity at the site of vessel injury<sup>17</sup>. Once thrombin is produced, it enters a feedback loop to activate factors VIII and V, converts fibrinogen to soluble fibrin monomers, and helps to stabilize the fibrin monomer by converting factor XIII to XIIIa, which crosslinks the fibrin monomers to form a stable fibrin polymer<sup>15</sup>. Fibrin polymerizes rapidly, forms the primary structure of the thrombus, traps platelets and erythrocytes, and binds circulating coagulation and fibrinolytic factors<sup>17</sup>. Within the platelet-rich fibrin clot, platelets continue to secrete their granule contents and growth factors, thus contributing to the advancement of the growing thrombus. Under certain conditions, an occlusive, platelet-rich thrombus can result.

Upon development of the fibrin clot, fibrinolysis is also initiated. Fibrinolysis, the physiological process for dissolving fibrin deposits, is the slow and progressive enzymatic cleavage of fibrin to soluble fragments. During any type of vascular injury, there is a parallel process of thrombosis formation and thrombolysis. Therefore, the ultimate extent of thrombus formation appears to be dependent upon the dynamic balance between factors that promote fibrin deposition and platelet activation, and factors that promote fibrinolytic activity<sup>17</sup>. Initially, early thrombus formations are caused by

platelet aggregation, but fibrin deposition from the coagulation cascade is responsible for thrombus stability <sup>9</sup>.

Before initiation of the common pathway via the intrinsic system, platelet membrane phospholipids are required. All factors necessary for fibrin formation within the intrinsic are in direct contact with or contained in the blood. Initiation of the intrinsic pathway is due to exposure to sub-endothelial components such as collagen, phospholipids, or kallikrein (activated Fletcher factor) activation of factor XII to XIIa. Since factor XII is only partially activated by contact with damaged vessel component, Fletcher factor and high molecular weight kinogen (HMWK) are required to amplify the contact activation for the formation of factor XIIa. Contact activation of the intrinsic system occurs in the absence of  $\text{Ca}^{2+}$ . In the presence of HMWK, factor XIIa transforms factor XI to XIa. Next, factor XIa converts factor IX to IXa in the presence of  $\text{Ca}^{2+}$ . Following conversion of factor IX, factor IXa along with the essential cofactor VIII:C in the presence of  $\text{Ca}^{2+}$  and PF3 (platelet factor 3), a source of membrane phospholipid, activates factor X to Xa <sup>16</sup>. The macromolecular complex of factors IXa, VIII:C, X, PF3, and  $\text{Ca}^{2+}$  organizes on the surface membranes of activated platelets <sup>15</sup>. The platelet membrane provides a protective environment that expedites the biochemical reactions of the intrinsic system without interference from physiological anticoagulants present in the plasma <sup>15</sup>.

The extrinsic system is initiated with the presence of tissue factor in the blood circulation. Tissue factor, also known as thromboplastin or factor III, is a membrane-associated glycoprotein (GP) expressed in atherosclerotic plaques by macrophages and possibly SMC <sup>17</sup>. Under normal conditions, tissue factor is isolated from circulating

blood, but during severe vasculature trauma, tissue factor leaks into the blood from cells extrinsic to blood vessels. Oxidized LDL has been shown to induce EC and monocytes to express increased levels of tissue factor, and it has been demonstrated by Drake and colleagues that there is abundant tissue factor in the intima of atherosclerotic lesions<sup>8</sup>. It is the phospholipid portion of tissue factor that is required for extrinsic pathway initiation. After exposure of tissue factor to the circulation from plaque rupture or endothelial damage, factor VII is activated to factor VIIa in the presence of tissue factor and ionized calcium ( $\text{Ca}^{2+}$ ), also referred to as factor IV. Following activation of factor VIIa, factor X is activated by  $\text{Ca}^{2+}$ , factor VIIa, and tissue factor to form factor Xa. The factor X/VIIa/tissue factor complex is regulated by circulating tissue factor pathway inhibitor<sup>17</sup>. Production of factor Xa, the final reaction of the intrinsic and extrinsic systems, is the starting point for the common pathway. The extrinsic pathway has fewer steps than the intrinsic system and occurs rapidly, within a matter of seconds. Thrombin generated by the extrinsic system can accelerate the intrinsic pathway by enhancement of factors V and VIII<sup>16</sup>.

## **1.2 Platelets and Their Role in Hemostasis**

Circulating platelets, also known as thrombocytes, are critical to the coagulation cascade for thrombus formation. Upon traversing an area of thrombotic activity, platelets are in a constant struggle between states of activation by agonists and inactivation by inhibitors. Only activated platelets are capable of thrombin generation from prothrombin. Before 1960, very little research was applied to understanding platelet function, but in

1962 Born devised a simple method for studying the response of platelets to added agonists by measuring changes in optical density <sup>18</sup>.

Platelets are smooth, disc-shaped anuclear cell fragments about 2 to 3  $\mu\text{m}$  across and shed from the cytoplasm of mature megakaryocytes. Two-thirds of the platelets released circulate in the bloodstream, while the remaining one-third is sequestered in the spleen at equilibrium with platelets in the blood. In the circulation, they number 130,000 to 400,000 per  $\text{mm}^3$  of blood. Platelets have an average lifespan of approximately ten days, and their structure can be divided into four distinct areas. These consist of the peripheral zone, sol-gel zone, organelle zone, and membrane systems. Figure 3 illustrates the major platelet divisions.

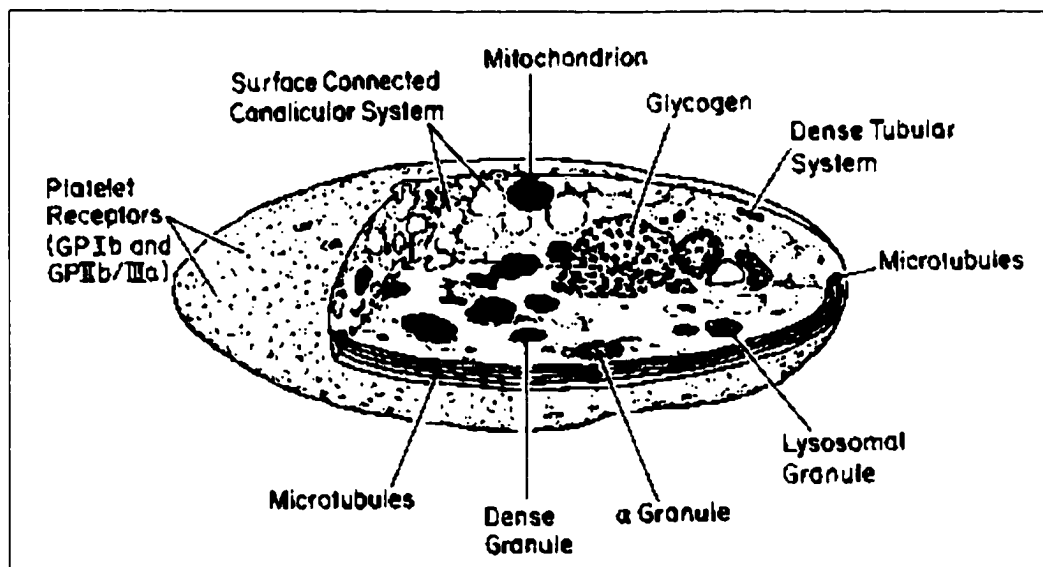


**Figure 3 – Major divisions and contents of a typical platelet  
(From Turgeon 15)**

The peripheral zone consists of the cytoplasmic membrane containing several glycoproteins surrounded by the glycocalyx, which contains absorbed coagulation proteins such as factor V, factor VIII, and fibrinogen. Integral glycoproteins, which serve

as receptors for external stimuli, are on the membrane surface as well as on the surface of interior membrane channels. Arachidonic acid, a precursor to TxA<sub>2</sub>, is a major component of the phospholipid portion of the platelet membrane. Major elements of the sol-gel zone consist of microtubules and microfilaments whose primary functions are to provide a cytoskeleton and contractile system. Increased intracellular Ca<sup>2+</sup> concentration induces contraction of the cytoskeleton during platelet activation.

Beneath the microtubule layer is the organelle zone, composed of mitochondria, glycogen particles, dense bodies, alpha granules, and lysosomal granules.

Dense bodies contain ADP, ATP, other nucleotides, phosphate compounds, Ca<sup>2+</sup>, and serotonin. ADP stored in the dense bodies is called the non-metabolic pool of ADP to distinguish it from the metabolic pool, which is found in the cytoplasm and used for aerobic metabolism<sup>19</sup>. Cytoplasmic ADP is used as energy for normal platelet metabolism, whereas the non-metabolic ADP is used during platelet aggregation. Alpha granules are the most abundant of the granules and contain vWF, fibrinogen, serotonin, factor V, factor VII, fibronectin, alpha<sub>2</sub>-antiplasmin, albumin, beta-thromboglobulin, platelet factor 4, and platelet derived growth factor (PDGF)<sup>19</sup>. Platelets contain two membrane systems called the open canalicular and dense tubular systems. The open canalicular is continuous with the platelet membrane, but the dense tubular system, which serves as a storage site for Ca<sup>2+</sup>, is not. Both membrane complexes appear to be important regulators of intracellular Ca<sup>2+</sup> concentration<sup>19</sup>.

In regard to platelets, thrombus formation takes place through orchestrated events involving adhesion, activation, primary aggregation, and secondary aggregation. Platelet adhesion occurs when the endothelial surface is interrupted, exposing substrates such as

collagen, vWF, fibronectin, vitronectin, and laminin. Initial platelet adherence is dependent upon plasma vWF binding to the injury site, done to possibly increase local vWF concentration <sup>11</sup>. vWF has been shown to bind to types I and III collagens, and it has been suggested that it also binds with type IV collagen. vWF present in the subendothelium can support about 40% of total platelet adhesion, but its concentration is not adequate enough for the optimal initiation of hemostasis <sup>3,11</sup>. Glycoprotein Ib (GPIb) is present on the platelet membrane in a tight complex with glycoprotein IX (GPIX). This GPIb-IX complex (about 25,000 copies per unstimulated platelet) mediates the initial adhesion of unstimulated platelets to vWF bound within the subendothelium of damaged vessels <sup>20</sup>. Other adhesive proteins of the subendothelium can mediate platelet adhesion, but under conditions of high shear flow, vWF appears to be absolutely required for platelet adhesion <sup>11</sup>. It has been shown that  $Ca^{2+}$  is not required for platelet adhesion to collagen.

The first characteristic of platelet activation is indicated by transformation from a discoid shape to a sphere with cytoplasmic projections protruding from the surface. All agonists that induce a platelet response initially cause this morphological change, but platelet shape change is a reversible process in the presence of weak agonists. A second characteristic of platelet activation is morphological changes within the glycoproteins on the membrane surface and glycocalyx. These changes cause the platelet to become sticky, and ligands can then attach to their membrane receptors to further stimulate the platelet and deliver chemical messages across the platelet membrane <sup>19</sup>. The immediate effect of all platelet agonists is similar, for cytoplasmic  $Ca^{2+}$  concentration is increased due to  $Ca^{2+}$  shift from the dense tubular system resulting in a decrease in cytoplasmic

cyclic AMP (cAMP), which causes additional  $\text{Ca}^{2+}$  mobilization. Four possible responses related to platelet activation are (1) shape change (2) aggregation (3) formation of  $\text{TxA}_2$  and (4) granule secretion. Agonists such as ADP and epinephrine are weak stimulators capable of inducing the first two responses, while collagen and thrombin are strong agonists that can potentially lead to all six responses <sup>19</sup>.

Secondary aggregation follows primary aggregation and is irreversible and is mediated by dense granule secretion and  $\text{TxA}_2$  generation. Platelet response to agonists is a graded process. As activation continues, contraction and pseudopod formation progress, constituents of the organelle zone are redirected towards the center of the platelet, and further contraction results in dense body and alpha granule expulsion into the open canalicular system, which transports contents to the extracellular fluid <sup>16</sup>. Secretion of dense bodies, alpha granules, and  $\text{TxA}_2$  amplifies the activation of adjacent platelets causing inter-platelet connections to develop via vWF and the GPIIb-IIIa receptor. Threshold values for platelets are listed in Table 1. The exposure of GPIIb-IIIa by platelet activation in the presence of  $\text{Ca}^{2+}$  allows fibrinogen as well as vWF to form links between platelets resulting in aggregates <sup>21</sup>. Each platelet contains about 40,000 GPIIb-IIIa receptors, the most abundant surface protein that accounts for about 15% of the protein mass of the platelet membrane <sup>22</sup>. GPIIb-IIIa also has binding sites for adhesive proteins such as fibrinogen, fibronectin, and vitronectin and is independent of platelet activation, but the binding of vWF to GPIIb-IIIa occurs only after platelet activation <sup>11</sup>. The number of fibrinogen molecules binding to GPIIb-IIIa expressed per platelet on the platelet surface can vary from 25,000 generated by weak activators, to about 80,000 for strong activators <sup>23</sup>.

**Table 1 – Threshold values of platelet agonists**

<b>Agonist Concentration</b>	<b>Effect</b>	<b>Reference</b>
ADP		
0.2 $\mu$ M	Shape change	24
1.0 $\mu$ M	Reversible aggregation	24
TxA2		
0.03 $\mu$ M	Shape change	24
0.20 $\mu$ M	Reversible aggregation	24
0.60 $\mu$ M	Irreversible aggregation	24
Thrombin		
0.1 units/mL	Irreversible aggregation	24
Serotonin		
5.0 $\mu$ M	Potentiates shape change	25

ADP released from dense granules and neighboring erythrocytes interact with platelet membrane glycoproteins to activate further GPIIb-IIIa receptors<sup>21</sup>. Further aggregation of surrounding platelets is secured through the release arachidonic acid from the platelet membrane. Arachidonic acid is released from the platelet membrane into the cytoplasm by the stimulatory activity of collagen, thrombin, ADP, and serotonin<sup>26</sup>. Through the cyclooxygenase and synthetase enzyme systems in the platelet, arachidonic acid is converted into TxA2, which promotes further aggregation and is a potent vasoconstrictor<sup>21</sup>. Serotonin in the concentration range of 0.3 to 0.6  $\mu$ M potentiates ADP-induced shape change, but serotonin alone as an activator is ineffective at these concentrations<sup>25</sup>. From recent experimental evidence, it has been suggested that serotonin dose-dependently enhances platelet activation induced by ADP and thrombin, thus supporting the idea of serotonin as a helper agonist<sup>27</sup>.

Mitogenic contents are also expelled from the alpha granules at the site of injury. Chemokines, mitogens such as PDGF, transforming growth factor beta, and basic fibroblast growth factor, stimulate the migration and proliferation of SMC from the

media to the intima and initiates the production of types I and III collagens, elastin, and glycoproteins<sup>10,20</sup>. It is probable that many of the growth factors have a synergistic role in promoting cell proliferation, while others may have an inhibitory effect<sup>1</sup>.

Platelet transport to the site of injury is influenced by wall shear stress, and high shear rates can activate and aggregate platelets in the absence of exogenous agonists. Shear rate ( $\text{sec}^{-1}$ ) is defined as how fast the adjacent fluent layers are flowing past one another, while shear stress is the force per unit area ( $\text{dynes/cm}^2$ ) the blood exerts on either blood constituents or the vascular wall in the direction of flow. In the 1970's, much research was performed on platelet function in relation to different shear stresses and shear rates. It was shown by Munter and Stein that at sufficiently elevated rates of shear, the shear rate versus shear stress relation for blood is identical to that of water, therefore implying that blood can be assumed to be a Newtonian fluid under certain conditions<sup>28</sup>. Blood is considered as a Newtonian fluid at shear rates above  $1000 \text{ sec}^{-1}$ <sup>29</sup>. Shear stress at low magnitudes has no measurable effect on platelets, but there are threshold values at which measurable changes of platelet response exist<sup>18</sup>. Several experiments have shown that the shear response and chemical response to agonists are highly synergistic. For example, Sutura *et al.*, subjected platelets to repeated, short duration pulses of exposure to shear stress with a one second pause between each pulse. It was observed that the pulsed exposure resulted in increased platelet aggregation over continuous exposure for the same total time. This experiment suggests that continuous exposure of platelets to stress produces a lower bound to the response of intermittent stress<sup>18</sup>. Shear enhanced mixing is the mode of convective transport by which platelets and plasma proteins interact with the vessel wall. Maximum platelet deposition was observed in

areas of flow recirculation and minimum in areas of elevated shear and flow separation<sup>30</sup>. In 1988, a study performed by Aarts *et al.* demonstrated that as shear rate increased in a laminar flow, platelets were increasingly expelled from center of the flow towards the wall, which resulted in an elevated platelet wall concentration<sup>31</sup>. Even under minimal shear conditions as low as 50 dynes/cm<sup>2</sup>, changes in platelet morphology and biochemistry were observed<sup>32</sup>. It has been observed that fibrin is more abundant in thrombi formed under low local velocities because reduced velocity enhances the accumulation of activated coagulation factors resulting in thrombin accumulation<sup>29</sup>. Shear-induced aggregation does not require fibrinogen, and shear stress stimulates arachidonic acid metabolism<sup>18</sup>. In severe atherosclerotic vessels, shear stresses may be as high as 1000 dynes/cm<sup>2</sup><sup>29</sup>.

Platelets are very complex due to their extrinsic and intrinsic means of activation, but certain biochemical agents found in the plasma and manufactured by platelets and the endothelium act to inhibit platelet activation and aggregation. Antithrombin III (AT-III), a circulating plasma protein present in human blood at a concentration of 4  $\mu$ M, inhibits thrombin activity after thrombin generation<sup>24</sup>. Due to AT-III activity, thrombin is unable to convert fibrinogen into fibrin. Just as AT-III attenuates a crucial component of the coagulation cascade, nitric oxide (NO) and prostacyclin (PGI<sub>2</sub>) generation affect platelets and the endothelium directly. NO and PGI<sub>2</sub> act synergistically through cAMP and cGMP dependent mechanisms<sup>33</sup>. NO is produced by the endothelium and platelets, while PGI<sub>2</sub> is produced by the endothelium. Using arachidonic acid from the endothelial membrane as a precursor, PGI<sub>2</sub> is synthesized in a way similar to that of platelet TxA<sub>2</sub> production. Although PGI<sub>2</sub> and TxA<sub>2</sub> are similar in structure, PGI<sub>2</sub> is a vasodilator and

the terminal guanidinium nitrogen of the amino acid L-arginine, yielding L-citrulline as potent inhibitor of platelet aggregation. Both TxA<sub>2</sub> and PGI<sub>2</sub> are representatives of an important homeostatic mechanism for the regulation of platelet aggregation and arterial tone <sup>34</sup>. As long as the endothelium is intact and PGI<sub>2</sub> is produced and secreted, platelet aggregation is limited in time <sup>16</sup>.

Platelet and endothelial derived NO is generated by the five-electron oxidation of the co-product <sup>35</sup>. The entire reaction is catalyzed by the Ca<sup>2+</sup>-dependent form of the enzyme NOS. Figure 4 illustrates the mechanism of NO production in mammals. NO is a lipophilic molecule that can freely diffuse across cell membranes, and it interacts with many metal and thiol containing molecules. Like PGI<sub>2</sub>, NO is also a potent vasodilator and inhibitor to platelet aggregation. Within the platelet and endothelium, NO interacts with the soluble guanylate cyclase (SGC) enzyme to induce a conformational change within the enzyme to stimulate the conversion of GTP to cGMP <sup>35</sup>. Increases in cGMP result in decreased intracellular Ca<sup>2+</sup> levels and the subsequent inhibition of platelet activation with subendothelial SMC relaxation <sup>37,38</sup>. Intact endothelium can spontaneously release NO, resulting in a basal concentration that may inhibit thrombus formation on healthy vasculature <sup>37</sup>. Basal levels of NO produced by platelets and the endothelium are generated continuously, but the presence of platelet agonists occurs only during periods of platelet activation.

The endothelium can produce 10- to 40-fold more NO than needed to activate SGC <sup>39</sup>. Combined with the NO produced by platelets, toxic levels of NO do not accumulate, but NO toxicity is most likely to result in the diffusion-limited reaction of NO with superoxide (O<sub>2</sub><sup>-</sup>) to produce the toxic oxidant peroxynitrite (OONO<sup>-</sup>) <sup>39</sup>. This

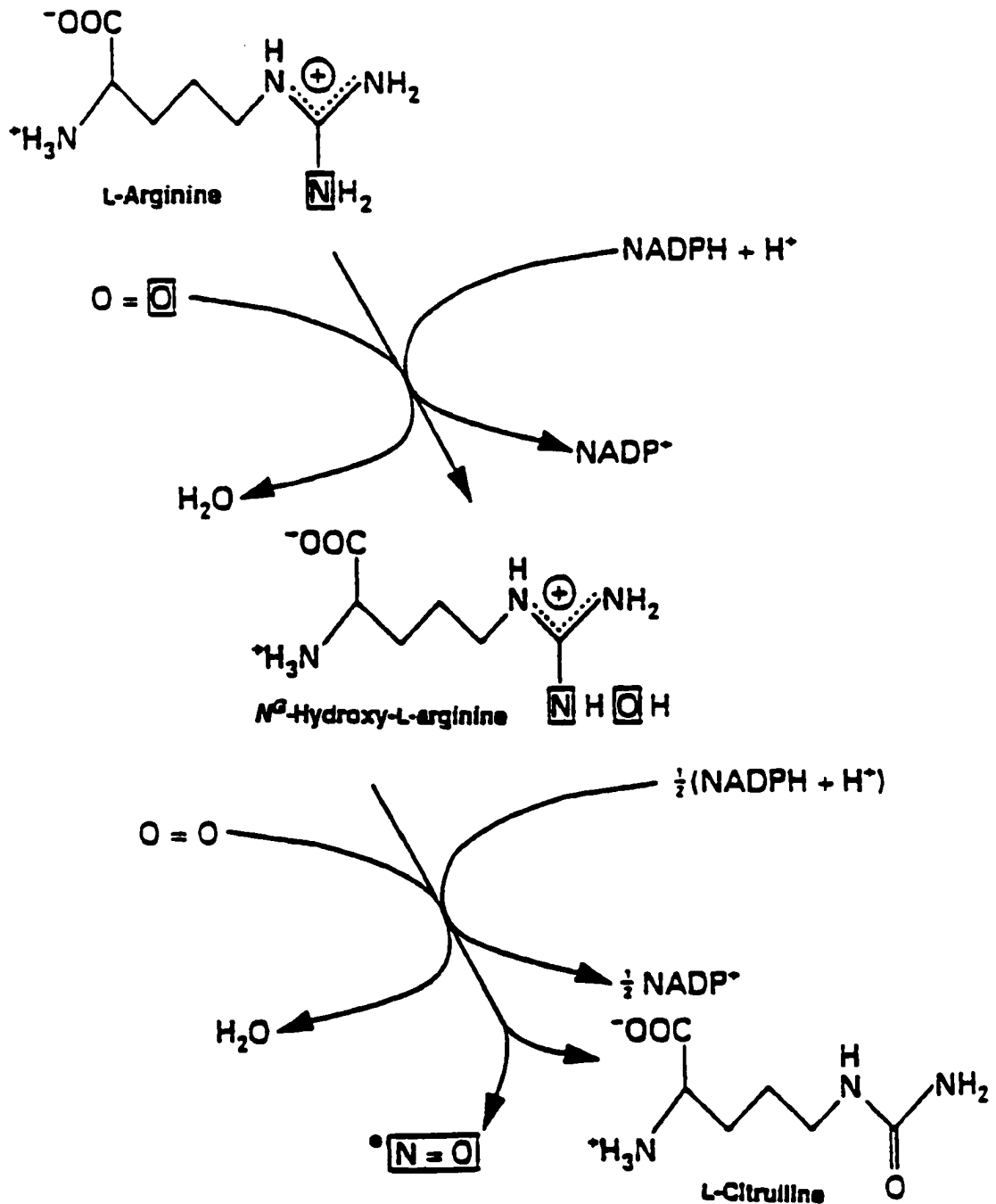


**Figure 4 - Overall reaction for the enzymatic production for NO (Adapted from Knowles *et al.* 36)** All NOS studied thus far generate NO for intracellular signaling or host defense by a 5-electron oxidation of one of the guanidino nitrogens of L-arginine. L-arginine,  $\text{O}_2$ , and  $\text{NADPH}$  are the reactants,  $\text{NO}$ , L-citrulline, and  $\text{NADP}^+$  are the products. It has been assumed (but not proven) that the chiral center of arginine retains its absolute configuration when converted to citrulline. The boxed O and N atoms show the origin of the constituent atoms of NO.

reaction ( $k = 3.7 \times 10^7 \text{ M}^{-1}\text{sec}^{-1}$ ) occurs spontaneously whenever NO and  $\text{O}_2^-$  are produced together. Nitrotyrosine, a marker of  $\text{OONO}^-$  oxidation of proteins, is noticed extensively in human atherosclerotic lesions<sup>39</sup>. Plasma does not consume NO, but oxyhemoglobin does, yielding methemoglobin and nitrate as reaction products. The ratios of rates of NO uptake and release for Fe(II)-hemoglobin is 5 to 6 orders of magnitude greater than that for oxygen<sup>40</sup>. Due to the high reactivity of NO with plasma constituents, NO must be present in sufficient quantities to counteract the effect of platelet agonists. Figure 5 illustrates the possible physiological reactions with NO.

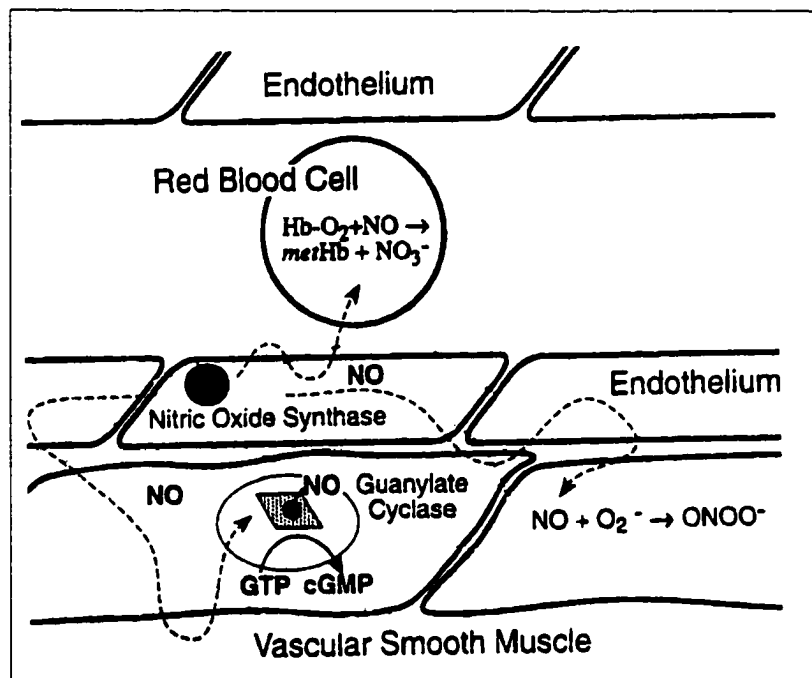


**Figure 5 - Biological reactions of nitric oxide**  
(Adapted from Beckman, *et al.* 39)

Biological reactions of NO can be simplified to three main reactions: (1) its activation of SGC (2) its destruction by reaction with oxyhemoglobin and (3) its reaction with  $\text{O}_2^-$ <sup>39</sup>. Mammalian systems express superoxide dismutase (SOD) and catalase activities to prevent toxicities, but SOD is far less efficient than NO as a scavenger of  $\text{O}_2^-$ <sup>39,40</sup>.

Superoxide concentration is kept relatively low by SOD, but there is a continual flux of  $O_2^-$  due to aerobic metabolism. About 1 to 5% of total oxygen inspired is reduced to  $O_2^-$  <sup>39</sup>. Due to its short half-life *in vivo*, NO does not react rapidly with most biological molecules. It does react with aqueous oxygen in a second order reaction with a half-life inversely proportional to initial NO concentration. Therefore, the half-life of NO increases as NO becomes more dilute. Physiological solutions containing NO range from a maximum of 4  $\mu$ M, the amount measured during cerebral ischemia, to a minimum of 5 nM, the amount needed to activate SGC <sup>39</sup>. For example, the half-life of NO for the 5 nM level is greater than 70 hours (solely reacting with  $O_2$ ), but in the presence of  $O_2^-$  and hemoglobin the half-life is less than a few seconds. In the past few years, much research has been performed on the functions of NO in biological systems. The physiological role of NO function can be tested through experimentation by providing competitive inhibitors to NO synthesis. Two compounds readily available from chemical supply companies are nitro-L-arginine methyl ester hydrochloride (L-NAME) and N<sup>G</sup>-methyl-L-arginine acetate salt (L-NMMA). Both compounds are fast acting and directly compete with L-arginine binding to NOS.

Knowledge of the local NO concentration, which minimizes platelet adhesion and aggregation at sites of vascular injury, would be useful for the design of NO-releasing biomaterials <sup>38</sup>. However, many past experiments and mathematical models pertaining to atherosclerosis and thrombus formation did not incorporate NO as an inhibitor of coagulation activity.

Through past experimental studies, much information has been attained on how platelets react with each other and the surfaces with which they come in contact.

Information obtained from these experiments warrants direct implementation into mathematical models for purposes of validation and extrapolation. Currently many models on platelet transport are founded upon chemical kinetics, diffusion, and hemodynamics. Sorensen *et al.* have recently developed and published a model based upon the concentrations of resting platelets, activated platelets, platelet-released agonists, platelet-synthesized agonists, prothrombin, thrombin, and AT-III <sup>41</sup>. With these minimal components, they were also able to show similar results obtained *in vitro* by Wagner and Hubbell <sup>42</sup>. Although this model demonstrated good agreement between the mathematical simulation and experiment, it was based upon a rectangular rather than cylindrical geometry and did not incorporate the inhibitor NO and agonists such as shear stress, O<sub>2</sub><sup>-</sup>, and serotonin. Analytical measurement of platelet-derived agonists and inhibitors are required for proper evaluation of a mathematical simulation.

### **1.3 Introduction to Voltammetry**

Voltammetry encompasses a group of electroanalytical methods in which information about a chemical species is derived from the measurement of current as a function of applied potential obtained under conditions that encourage polarization of a working electrode <sup>43</sup>. Historically, voltammetry developed from polarography, which was discovered by the Czechoslovakian chemist Jaslav Heyrovsky in the early 1920's <sup>43</sup>. Recent advances in microelectrode technology have enhanced the resolution and sensitivities of the working electrodes. Use of voltammetry is limited to compounds that are electrochemically reducible or oxidizable. Voltammetric methods commonly used for the *in vivo* and *in vitro* detection of biological compounds are cyclic voltammetry

(CV), chronoamperometry (CA), and differential pulse voltammetry (DPV). Proper selection of technique is dependent upon the analyte of interest. Sub-sections 1.3.1 to 1.3.3 briefly review the advantages and disadvantages of each technique.

### **1.3.1 Cyclic Voltammetry**

In CV, the working electrode's current response is excited by a triangular potential waveform (versus reference electrode). From a predetermined starting potential, the voltage is varied linearly to a maximum potential whereupon the scan direction is reversed until the potential is restored to the starting potential. This scan procedure can be repeated several times with cycle times ranging from 1 msec to 100 seconds or more. Time between scans is usually 10 times the duration of the voltage scan to allow the diffusion layer to relax to its original state<sup>44</sup>. Advantage to using CV is the time resolution that can be obtained from running fast successive scans, allowing insight to diffusion processes and chemical kinetics. Detection limitations in CV are due to interference by current (residual current) other than the electrochemical reaction (faradaic current) of interest. Residual current is associated with electrode surface properties (capacitance charging) and increases linearly with scan rate, whereas the faradaic current increases with the square root of scan rate because of its association with diffusion<sup>44</sup>. Detection limits for CV are on the order of 50 nM<sup>45</sup>.

### **1.3.2 Chronoamperometry**

In CA, the working electrode potential is held constant and current is measured as a function of time. Excellent temporal resolution is achieved with this technique, and the current measured throughout the measurement interval is proportional to the concentration of the species oxidized or reduce. CA is the most sensitive voltammetric

technique with a low-level detection limit in the sub-nanomolar range <sup>46</sup>. The main disadvantage to this technique is that the origin of the current can no longer be discriminated. In a multiple species system, the measured current is a superposition of any species that is electrolyzed at or below the working electrode potential.

### **1.3.3 Differential Pulse Voltammetry**

DPV was developed to provide high discrimination against residual current and is a hybrid of CV and CA <sup>44</sup>. This technique has a detection limit around 5 nM, but sensitivity is achieved through loss of time resolution. The potential applied to the working electrode is a linearly increasing pulse train, which is illustrated in Figure 6. In DPV, the difference in current per pulse is recorded as a function of a linearly increasing voltage. Current is measured at two points for each pulse, the first point just before the application of the pulse and the second at the end of the pulse. These sampling points are chosen to allow for the decay of the residual current. This technique results in a curve consisting of a peak that is directly proportional to concentration.

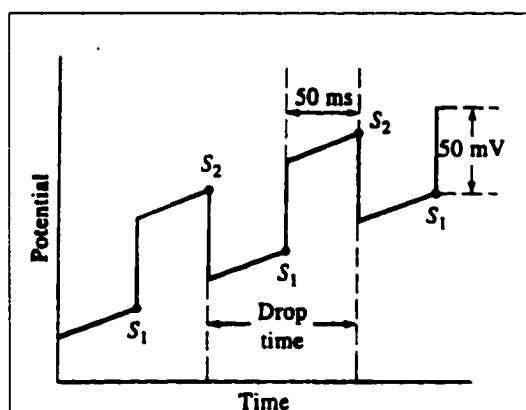


**Figure 6 – Working electrode potential in differential pulse voltammetry  
(Adapted from Skoog *et al.* 43)**

For reversible reactions, the peak potential is approximately equal to the standard potential for the half reaction (half-wave potentials are useful for discrimination of chemical species). DPV allows concentration discrimination for different species in solution whose half-wave potentials differ by as little as 40 to 50 mV, whereas classical and normal pulse techniques require a potential difference of about 200 mV for resolution of multiple species<sup>43</sup>. Figure 7 compares DPV with classical voltammetric techniques.

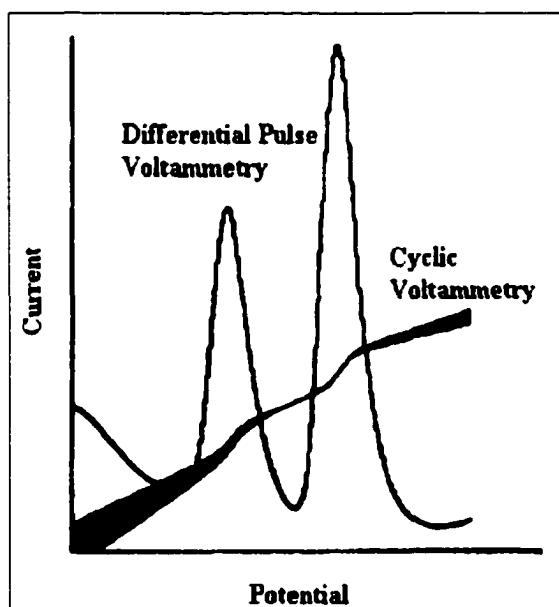


**Figure 7 – Differential pulse voltammetry compared to cyclic voltammetry (Adapted from Princeton Applied Research, application note 155)**

### **1.4 Hypothesis and Specific Aims**

Nitric oxide (NO) has been shown to suppress platelet activation, induce vasodilation, inhibit smooth muscle cell proliferation, and act against infection. Activated platelets generally have opposite effects from these. They secrete platelet-derived growth factor (PDGF), which stimulates smooth muscle growth; serotonin, which is a platelet agonist; and a number of agents that promote further platelet aggregation.

However, activated platelets also produce NO through the enzymatic functions of the constitutive form of nitric oxide synthase (NOS). The primary functions of this capability are not yet completely understood. Due to its low molecular weight and high diffusivity, NO is quickly transported from its source to surrounding tissues and medium, and this characteristic may be instrumental to its function. Understanding the way in which NO interacts with platelet function could assist in the development of improved diagnostic and surgical procedures as well as biomaterials that are resistant to thrombus formation. Due to the short half-life of NO *in vivo* and *in vitro*, it is desirable to use platelet-derived serotonin and an indicator for NO function. Currently, highly sensitive electrodes are available which allow real-time electrochemical measurement of serotonin. The purpose of this doctoral project is to apply this electrode to an *in vitro* blood model to test the following hypothesis.

#### **1.4.1 Hypothesis**

Serotonin expelled from activated platelets upon exposure to fibrillar collagen is influenced by platelet-derived nitric oxide.

#### **1.4.2 Study Objectives**

The objective of this study is to develop mathematical simulations and an *in vitro* model that represents the concentrations of platelet agonists and inhibitors using bovine blood. All results will be tested for statistical significance against a control.

Specific objectives are as follows:

1. To compare and contrast concentration profiles of NO and platelet-derived agonists in a static mathematical simulation

2. To electrochemically measure serotonin concentration in real-time during *in vitro* aggregation of platelets to fibrillar collagen in a static situation with and without a NOS inhibitor
3. To verify the degree of platelet adhesion to fibrillar collagen in part 2 through histological analysis

## CHAPTER 2

### MATERIALS AND METHODS

#### 2.1 Mathematical Models

##### 2.1.1 Introduction to Mathematical Models

Through the use of mathematical models it was desirable to simulate the static diffusion of platelet-derived agonists and inhibitors with a transient one-dimensional analysis. Due to the low concentrations involved, it is difficult to measure agonist and inhibitor concentrations near a surface where a platelet thrombus exists<sup>25</sup>. Therefore, the use of mathematical models is warranted. Agonist and inhibitor release information from the literature was used as starting parameters for mathematical simulations. Table 2 indicates the species of interest for the mathematical analysis, their origin, and action.

**Table 2 – Species and inhibitors of interest for mathematical modeling**

<b>Species</b>	<b>Action</b>	<b>Origin</b>
ADP	Activator	Dense granules
TxA2	Activator	Platelet membrane
Thrombin	Activator	Platelet membrane
NO	Inhibitor	Platelet membrane
Serotonin	Activator	Dense granules
AT-III	Inhibits Thrombin	Plasma
O <sub>2</sub> <sup>-</sup>	Inhibits NO	Plasma

For this dissertation, two separate models were developed for diffusion in a static medium. The first model simulates agonists and inhibitors generated by the platelet,

whereas the second model simulates agonists released by the platelets. The rate of species liberation and the diffusive transport from the surface determine the magnitude of the local agonist and inhibitor concentrations<sup>47</sup>. Although the governing equations for each model are similar, boundary and initial conditions--and hence solution methods--are different. Insights gained from the mathematical models allowed for the determination of theoretical bounds for agonist and inhibitor concentrations of interest. The following section discusses the development of the governing equations.

### **2.1.2 Model Assumptions**

Before development of the two mathematical models, assumptions were made concerning the diffusion of platelet-derived agonists and inhibitors. The models are designed to simulate the concentration profiles of agonist and inhibitors following *in vitro* platelet activation by collagen in a cylindrical coordinate system. Geometries for both models consist of a cylindrical dish whose surface is uniformly coated with collagen. The dish has a radial dimension of R, an infinite height of H, and blood plasma is assumed to be the medium for species transport. Figure 8 illustrates the physical parameters for mathematical modeling. The process of diffusion is assumed to follow Fick's first law of diffusion, which states that a species diffuses as a result of a concentration gradient in the direction of decreasing concentration<sup>48</sup>. Mathematically, this definition relates the mass flux of a species directly to its concentration gradient by the following equation where  $N_A$  is the species flux,  $D_{AB}$  is the diffusion coefficient

$$N_A = -D_{AB} \nabla C_A \quad \text{Eq. 1}$$

(assumed to be a constant) of species A in plasma, and  $\nabla C_A$  is the concentration gradient.

A transient analysis is assumed, and diffusion occurs primarily in the axial direction (z-

coordinate) which is space averaged over the radial and angular coordinates ( $r$  and  $\theta$ ). Any reactions occurring at the collagen surface are assumed to be heterogeneous. For certain agonists and inhibitors, consumption of the species occurs in the static plasma through zero- and first-order chemical kinetics. It is assumed that the plasma is initially void of the species of interest before platelet activation by collagen. Knowing the assumptions for mathematical modeling, the differential shell balance method can be employed for development of the governing partial differential equation. As mentioned before, model development is similar for both the agonist and inhibitor release and agonist generation models.

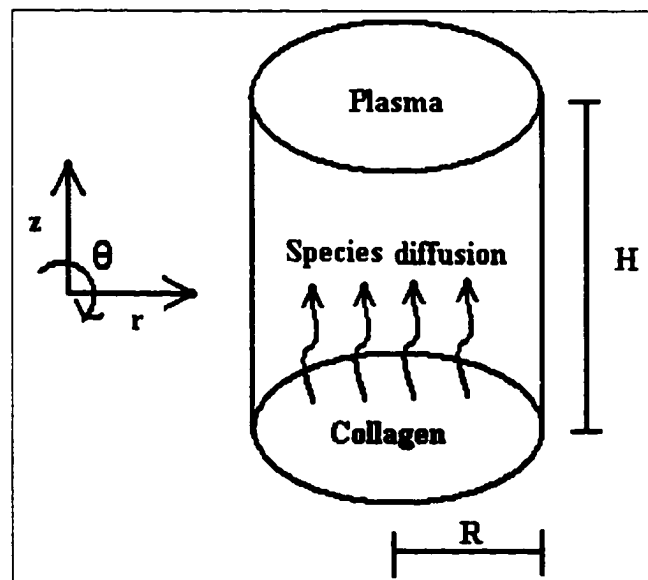


**Figure 8 – Physical parameters for mathematical model development**

### **2.1.3 General Model Development**

An appropriate differential shell was chosen based on the assumptions in the preceding section. Performing a conservation mass balance over a differential shell of plasma develops the governing equation. The mass balance states that the resulting concentration of an agonist or inhibitor within the differential plasma shell is equal to the

difference between the diffusive flux of the species into the shell, and the sum of the species lost due to consumption or diffusive flux out of the shell. Figure 9 illustrates the mass fluxes and consumption occurring within the plasma shell. In this figure,  $N_A$

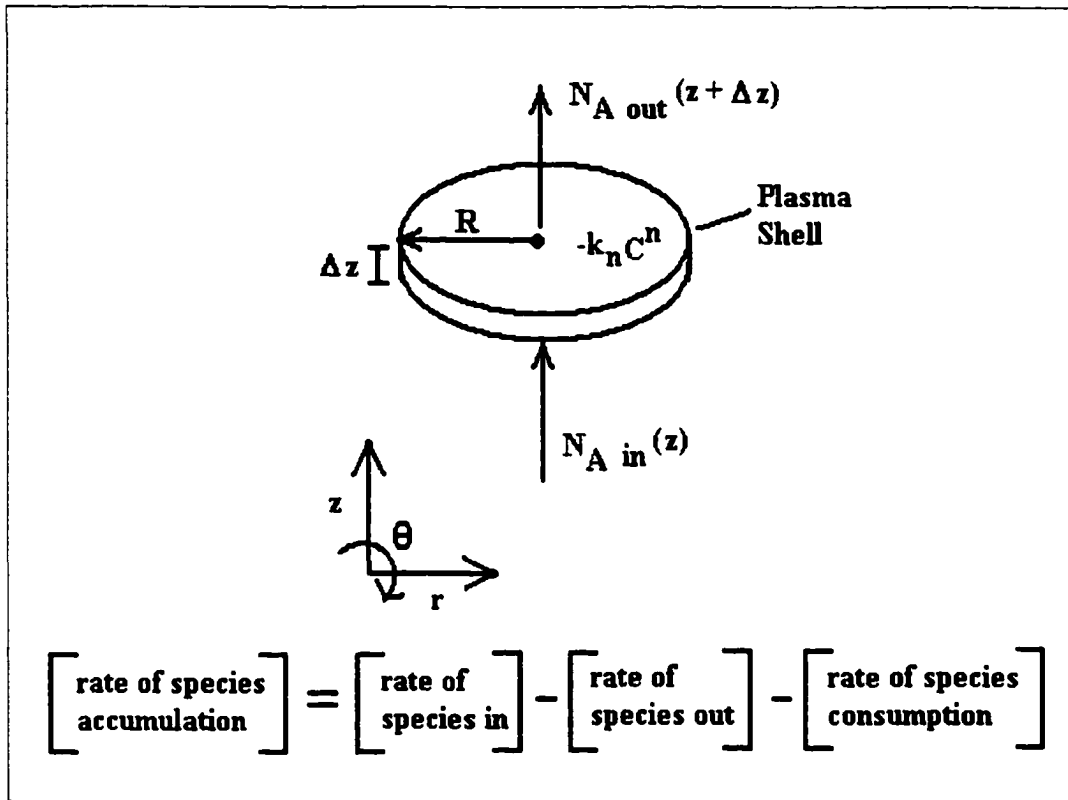


**Figure 9 – Species mass balance for a differential shell with consumption**

represents the mass flux of species A and  $-k_n C^n$  represents the homogeneous consumption reaction of order n, where k is the reaction rate constant. The reaction term can be transformed into a first-order reaction by assuming constant  $O_2^-$  and AT-III concentrations.

When the species are related as mass fluxes to the finite differential shell a mathematical expression (Eq. 2) is achieved that represents the diffusive transport.

$$\Delta z (\pi R^2) \frac{\partial C_A}{\partial t} = N_{A,z} \pi R^2 - N_{A,z+\Delta z} \pi R^2 - \Delta z (\pi R^2) k_n C_A^n \quad \text{Eq. 2}$$

This expression is transformed into a partial differential (Eq. 3) equation when the dimensions of the shell become infinitesimally small and Fick's law is applied.

$$\frac{\partial C_A}{\partial t} = D_{AB} \frac{\partial^2 C_A}{\partial z^2} - k_n C_A^n \quad \text{Eq. 3}$$

Upon integration of the resulting partial differential equation and application of boundary and initial conditions, a particular solution to the diffusion problem is obtained. The resulting solution for the platelet agonists and inhibitors is dependent upon whether they are generated on the platelet surface or released by the dense granules.

#### **2.1.4 Solution to Agonist and Inhibitor Generation Model**

Using Equation 3, and applying the proper boundary and initial conditions, the particular solution of the agonist generation models is developed. With species generation, it is assumed that generation occurs within or on the platelet phospholipid membrane. The two boundary conditions for this model are: (1) a constant heterogeneous flux ( $K$ ) of species at the collagen surface and (2) species concentration approaches zero at an infinite distance away from the collagen surface. An infinite distance was assumed to be on the order of a few millimeters distance, a valid assumption due to the platelets small size. The initial condition states that species concentration is equal to zero at all distances initially. Equations 4 through 6 below express these conditions mathematically.

$$-D_{AB} \frac{\partial C_A(t,0)}{\partial z} = K \quad \text{Eq. 4}$$

$$C_A(t, \infty) = 0 \quad \text{Eq. 5}$$

$$C_A(0, z) = 0 \quad \text{Eq. 6}$$

Agonists generated that are of interest for this model are thrombin and TxA2, while the inhibitor of interest that is generated is NO. Each of the species generated by the platelet is homogeneously consumed in the plasma. A Laplace transform approach through the application of equations 4 through 6 was used to find the particular solution for equation 3, which is represented by equation 7 below. The full solution to the problem is shown in appendix A.

$$C_A(t, z) = \frac{K}{\sqrt{\pi D_{AB}}} \int_0^t \frac{e^{-\left[ku + \frac{z^2}{4D_{AB}u}\right]}}{\sqrt{u}} du \quad \text{Eq. 7}$$

### **2.1.5 Solution to Agonist Release Model**

Solution to the agonist release model requires different boundary and initial conditions than the generation model. With agonist release, it is assumed that platelets release their granule contents immediately upon activation by collagen. The two boundary conditions for this model are (1) the flux at the collagen surface is zero for all time and (2) agonist concentration approaches zero at an infinite distance away from the collagen surface. Initial condition states that at time equal to zero, there is an impulse (represented by the Dirac delta function,  $\delta(z)$ ) of agonist release ( $m_0$ ) occurring only at the collagen surface. This condition implies that released agonists are initially concentrated in an infinitesimal zone near the surface of adhered platelets. Equations 8 through 10 express these conditions mathematically.

$$-D_{AB} \frac{\partial C_A(t, 0)}{\partial z} = 0 \quad \text{Eq. 8}$$

$$C_A(t, \infty) = 0 \quad \text{Eq. 9}$$

$$C_A(0, z) = \delta(z)m_0 \quad \text{Eq. 10}$$

Released agonists of interest for this model are serotonin and ADP. These are relatively stable and are therefore not consumed in the plasma. Modification to the governing equation is achieved by setting the consumption term equal to zero. A Fourier transform solution through the applications of equations 8 through 10 was used to find the particular solution, represented by Equation 11 below. The full solution to the problem is shown in Appendix B.

$$C_A(t, z) = \frac{m_0}{2\sqrt{\pi D_{AB}t}} e^{-\frac{z^2}{4D_{AB}t}} \quad \text{Eq. 11}$$

## **2.2 Preparation of Serotonin Sensor**

### **2.2.1 Sensor Design and Fabrication**

The sensor was designed to be sensitive to low concentrations of serotonin in a small volume of space. This type of sensor was carbon-fiber based and mounted on the tip of a pulled glass capillary tube for the purpose of serotonin detection *in vitro*. Production of the sensor is achieved with a four-step process. The first step involves the pulling of a glass capillary over a Bunsen burner flame.

A 50 mm glass capillary tube (Kimax®, Kimble Products) with a 1.5 mm internal diameter was used to create a tapered-tip glass capillary. The glass capillary was held between the thumb and forefinger of each hand, and the center of the capillary was slowly lowered onto the tip of the Bunsen flame (not directly within the flame). Holding the capillary tube in tension over the heat of the flame allowed the glass capillary to be pulled into two separate tapered-tip capillaries with sealed tips. Once the glass capillary cooled to room temperature, a razor blade was used to cut an opening on the narrowest

part of the tapered tips. The resulting tip was measured with a light microscope (Nikon® Instruments) to be approximately 200  $\mu\text{m}$ . Then, the freshly cut tips were quickly passed through the Bunsen flame (fire-polished) to smooth the sharp glass edges that resulted from cutting the tip.

The second step involved mounting the carbon fibers into the finished glass capillary tubes. Medical-grade carbon fibers (Amoco Performance Products, Greenville, SC, 6  $\mu\text{m}$  diameter, 12  $\Omega\text{-cm}$ ) were used as the sensing element for the serotonin sensor. The carbon fibers were shipped braided in a spool and had to be separated into individual fibers. Under sterile conditions using latex gloves, a 3-inch segment of braided fibers were cut from the spool and teased apart with a sterile probe. Once two individual fibers were isolated from the braid, they were gently twisted together to form a double fiber. It should be noted that although the carbon fibers are very strong, they are extremely brittle. Great care should be exercised during the entire fabrication process. Next, the twisted double fiber is loaded and gently advanced through the large diameter end of the tapered glass capillary until the double fiber can be seen protruding through the tapered end. Figure 10 illustrates the main parts of the sensor fabrication process.

The third step of the fabrication process involved creating an electrical contact for interfacing the transducer with supporting instrumentation. One end of a 1 to 2 m spooled bare copper wire (AWG 18, ARCOR®, Glenview, IL) was placed in a vise and pulled to straighten out any curvature or kinks. The straightened copper wire was then cut into 75 mm lengths and polished with fine-grain sandpaper to help increase the sensitivity and conductivity of the finished sensor. Then the polished 75 mm length of straight copper wire was covered entirely with a thin coat of conductive silver-epoxy (AI

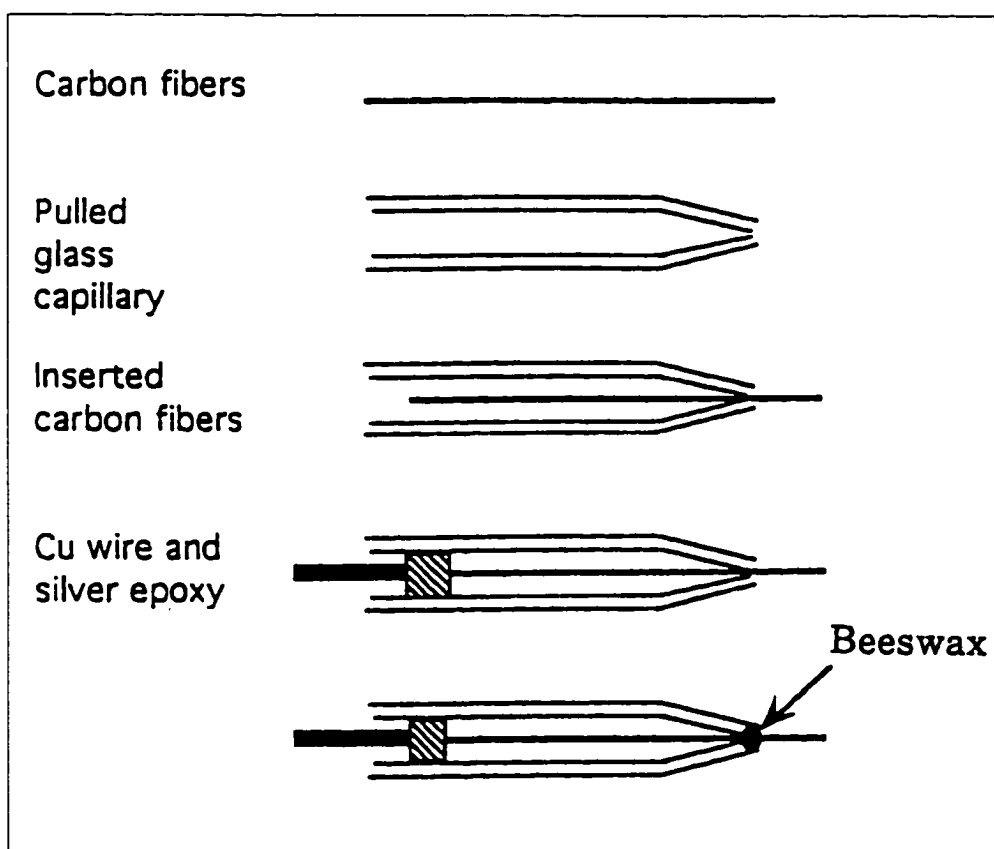


**Figure 10 – General fabrication process of serotonin sensor**

Technology, Lawrenceville, NJ) and was gently brought into contact with the carbon fiber protruding from the large diameter end of the tapered glass capillary. With the carbon fiber adhered tip. The fourth step involved the finishing procedure for the electrodes. After inserting the copper rod, the electrodes were baked in an oven at 100 degrees C for an hour to allow proper drying and curing of the silver epoxy. The baked electrodes were allowed to cool to room temperature, and then the protruding carbon fibers were trimmed with a new razor blade to a final length of 2.0 mm. Next, touching a drop of molten beeswax to the opening of the tapered tip, where the carbon fiber protrudes, sealed the tip of the glass capillary. After cooling, excess beeswax (a high molecular-weight ester) was removed by saponification (immersion in 0.1 M NaOH

overnight), followed by rinsing with distilled water. After rinsing, the finished electrodes were stored dry in a dust-free environment by inserting the copper conductor into a block of cork and covering with a 200 mL flask.

### **2.2.2 Supporting Instrumentation and Operation**

A Princeton Applied Research model 263A potentiostat/galvonostat (EG&G Instruments, Inc., Tennessee), interfaced to a PC-compatible Pentium computer through a GPIB port running the m270 electrochemical analysis software package (Princeton Applied Research), was used for the amplification and pre-processing of the electrode signal. All electrochemical measurements incorporated a three-electrode system consisting of a working electrode (carbon fiber sensor), a platinum-wire counter electrode, and a reference electrode. All three electrodes were in close proximity of (5 to 10 mm) of each other, but not touching.

The reference electrode (see figure 11) consisted of an isolated silver-silver chloride (Ag/AgCl) electrode (Ag/AgCl electrode obtained from World Precision Instruments). Isolation was achieved via a potassium chloride (KCl) salt bridge. This electrode was fabricated by the following procedure with reagents purchased from Sigma. A 4% agarose gel was prepared by dissolving agarose into KCl (40 mg/mL). The mixture was heated in a double boiler until all agarose was dissolved. Once it was dissolved, a plastic transfer pipette was attached to the end of a 1.0-inch length of Tygon tubing (1.5mm inside diameter). The end of the tubing was immersed into the dissolved agarose solution, and slight suction was applied to fill the volume of the tubing with the resulting agarose gel. After cooling, the agarose gel solidified and was ready for insertion into the Ag/AgCl electrode. Electrical contact between the KCl salt bridge and

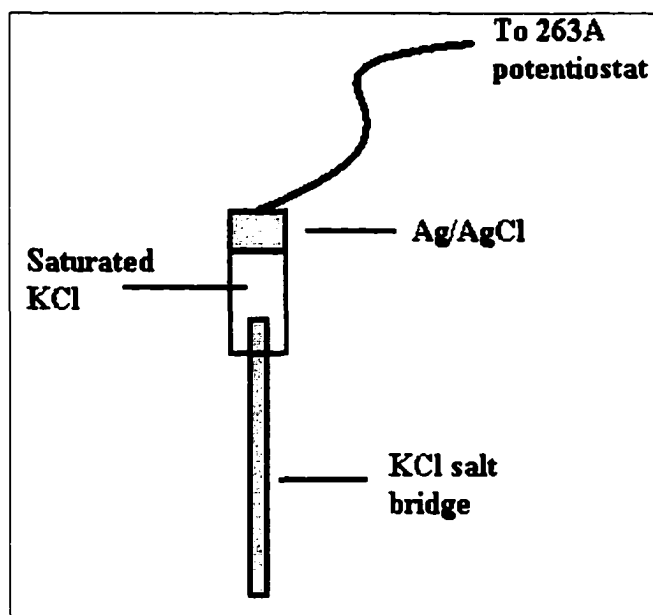


**Figure 11 – Isolated Ag/AgCl reference electrode**

Ag/AgCl electrode was achieved through a saturated KCl solution. When not in use, the reference electrode's tip was kept immersed in saturated KCl at room temperature to keep from drying. Reference electrode life was approximately three months if proper care was given.

Differential pulse voltammetry (DPV) was the method of choice for determination of serotonin concentrations. Figure 12 illustrates the parameters used for the DPV analysis. For calibration and experimental use, the voltage sweep for the DPV procedure was isolated to encompass the range where serotonin is oxidized and the range set from 300 mV to 700 mV with a scan rate and scan increment of 10 mV/sec and 3 mV respectively. The pulsing parameters were a pulse height of 25 mV, a step/drop time of 100 msec, and a pulse width of 50 msec. Importance of the pulse shape was explained in section 1.3.3 of chapter 1.

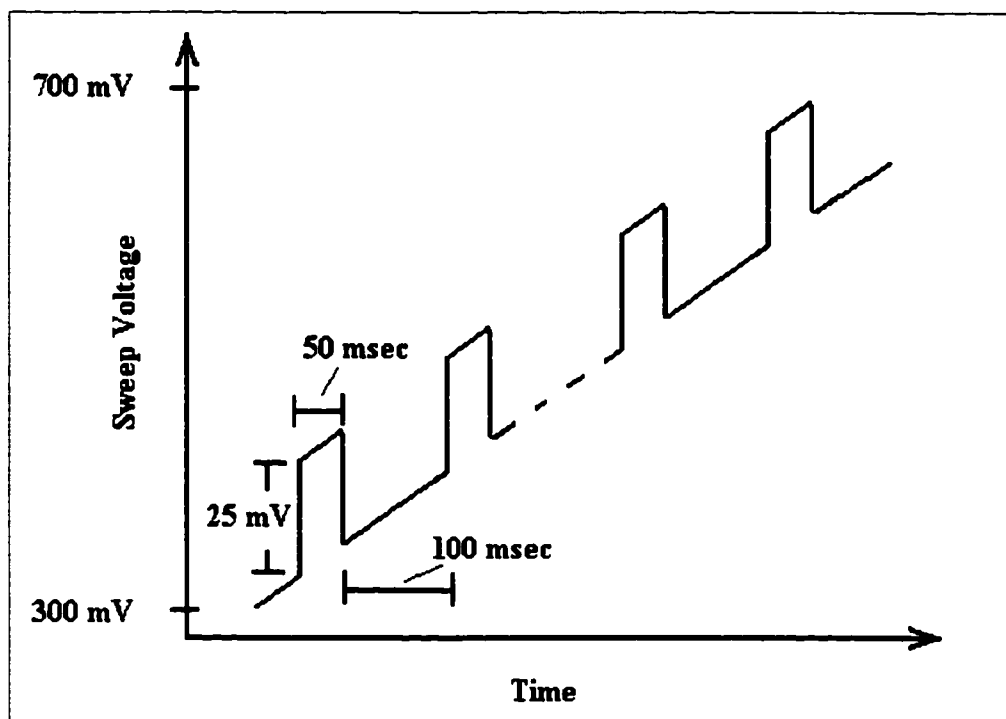


**Figure 12 – Differential pulse voltammetry parameters for serotonin detection**

## **2.3 Microelectrode Calibration and Analysis**

### **2.3.1 Preparation of Phosphate Buffer**

A phosphate-buffered saline (PBS) solution was the electrolytic medium for the calibration procedure. The basis of the PBS solution consisted of PBS tablets obtained from Sigma. To create 200 ml of PBS, one tablet was dissolved into 200 mL of distilled water. To match the pH and chemical environment the probe would be in contact with during experimental procedures, the PBS solution was made according to the procedure used by Volf *et al.* This solution was similar to a Tyrode buffer containing 137 mM of NaCl, 2.7 mM of KCl, 11.9 mM of NaHCO<sub>3</sub>, 1.0 mM of MgCl<sub>2</sub>, 0.42 mM of NaH<sub>2</sub>PO<sub>4</sub>, 5.5 mM of D-glucose, and 1.0 mM of CaCl<sub>2</sub> <sup>49</sup>. The buffer was also loaded with L-

arginine to create a final concentration of 1 mM. All reagents used were purchased from Sigma, and solution pH was adjusted to 7.4 by adding drops of either 0.1 M HCl or 0.1 M NaOH. Final solution pH was verified with pH sensitive paper. When not in use, the PBS solution was kept refrigerated and slowly heated to room temperature prior to use. Before each use, the pH was re-tested to ensure proper range ( $7.4 \pm 0.2$ ).

### **2.3.2 Electrochemical Pre-Treatment**

The surfaces of graphitic materials such as carbon fibers are very complex. Figure 13 illustrates the surface of a typical graphitic carbon surface. At the atomic level, graphite has a uniform structure (basal plane) and is almost electrochemically inert in aqueous solution. It appears that most electron transfer reactions occur at the edge of the basal plane, which is often covered with a large number of oxygen-containing function groups such as phenols, carbonyls, carboxylic acids, and quinones<sup>44</sup>. In 1980, Gonon and coworkers showed that an increased response from carbon fibers could be achieved through the electrochemical oxidation of the cylindrical surface<sup>50</sup>. Following treatment voltammograms appear sharper and the detection limit of some chemical species can approach 5 nM<sup>51</sup>.

Using the pre-treatment procedure outlined by Lantoine *et al.*, electrodes were conditioned with three electrochemical processes to ensure electrode stability and a reproducible baseline. They were treated in PBS solution by (1) applying an alternating potential frequency (50 Hz) of a triangular waveform for 20 seconds with the lower and upper potentials of the waveform being 0 V and 2.9 V respectively (2) applying a constant negative potential of  $-0.8$  V for 5 seconds and (3) applying a constant positive

potential of 1.5 V for 5 seconds<sup>52</sup>. Procedures for electrode conditioning were programmed into the model

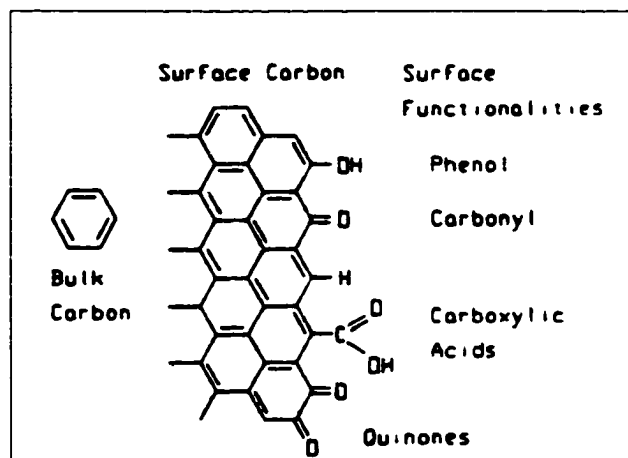


**Figure 13 – Graphitic oxide surface structures found on carbon materials (from Kawagoe, *et al.* 44)**

263A voltammetric analyzer using the m270 software. Electrode conditioning was conducted before any calibration or experimental use.

### **2.3.3 Creation of Serotonin Standards**

Serotonin (creatine sulphate complex, MW of 387.4, H-7752, 1 gm) was purchased from Sigma. Although serotonin is relatively stable at physiological pH and temperature, Sigma recommends that new standards be created before any use. Initially, a 400  $\mu\text{M}$  solution of serotonin was created (6.2 mg of serotonin into 40 mL PBS). This solution was then diluted with PBS to achieve 10 mL of a 40  $\mu\text{M}$  working standard (1 mL of 400  $\mu\text{M}$  serotonin solution into 9 mL of PBS). Between uses, the working standard was kept in the refrigerator or in an ice bath. To achieve the desired concentration of serotonin, microliter aliquots were injected with a Hamilton micro-syringe into a 35 mm polystyrene Petri dish containing 5 mL of PBS. For calibration purposes, the domains of serotonin concentrations were between 4 and 140 nM. Table 3 indicates the volume of

serotonin to inject into 5 mL of PBS to achieve a controlled concentration of serotonin for sensor calibration.

**Table 3 – Creation of 5 mL serotonin standards for calibration**

<b>Volume of 40 <math>\mu</math>M Required (<math>\mu</math>L)</b>	<b>Serotonin (nM)</b>
0.5	4.0
1.0	8.0
3.0	24.0
8.0	64.0
18.0	144.0

### **2.3.4 Calibration Protocol**

Electrode calibrations were necessary for finding a relationship between measured current and serotonin concentration. As mentioned before, a three-electrode system was implemented for serotonin detection. Sterile polystyrene tissue-culture dishes (35 mm x 10 mm, Corning) were the electrochemical cell for the calibration procedure. A new dish filled with fresh PBS was used for each electrode calibrated. Before the electrode system was placed into position, each electrode was rinsed three times with distilled water for the removal of any surface particles. The isolated reference was secured by a clamp to position just below the PBS surface, while the carbon fiber and platinum counter electrodes were secured with a micromanipulator above. Initially, the counter and working electrodes were held in a position above the PBS surface. Before execution of the DPV protocol, the counter and working electrodes were slowly lowered with the micromanipulator to a position just below the PBS surface. Figure 14 illustrates the physical setup for the calibration procedure. Calibration procedures were performed under a constant stir condition using a magnetic stirrer bar to ensure proper mixing of the PBS with serotonin.

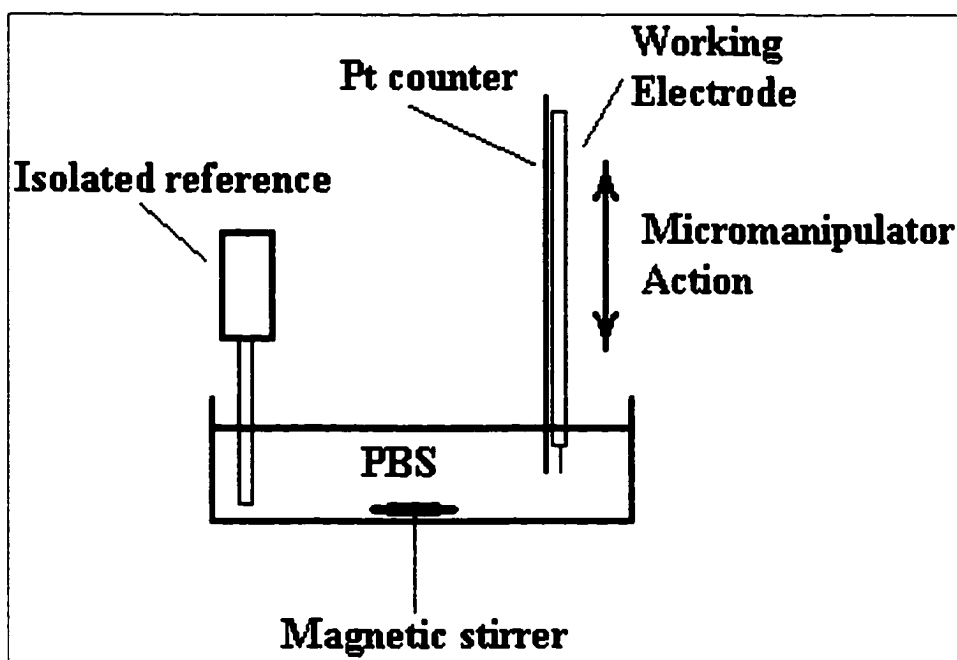


**Figure 14 – Electrochemical cell used for electrode calibration**

All probes were calibrated with serotonin concentrations of 0, 4, 8, 24, 64, and 144 nM respectively. A serotonin concentration of zero represented a baseline measurement taken solely in PBS. For each serotonin concentration, three repeated measures were performed, and the raw data acquired by the potentiostat was saved as an ASCII text file and stored on the computer's hard drive for post-processing. Including the baseline measurements, a total of 18 files were saved for each probe calibrated (3 repeated measures, 6 different concentrations). Raw data consisted of current in nA versus scan potential in mV.

### **2.3.5 Analysis of Sensor Data**

Raw data obtained from the DPV procedure were post-processed using Labview 5.1 software (National Instruments, Austin). A Labview virtual instrument was developed to read the raw DPV data for an entire electrode calibration, calculate the changes in signal currents attributed to serotonin oxidation occurring at  $550 \pm 50$  mV,

and save the processed values as a function of calibration concentration within a Microsoft Excel spreadsheet file. Change in current was calculated as the magnitude of the difference between baseline and oxidation peak.

Due to inherent Gaussian noise in the raw data, oxidation peaks were modeled as fourth-order polynomials, with the peaks considered to be the relative minima of the functions. Baseline levels were determined to be the average of five data points before baseline deflection caused by serotonin oxidation. Figure 15 illustrates how the analysis is performed on a single raw data file. Important parameters saved to the spreadsheet file consisted of the of magnitude of current difference between peak and baseline, relative minima potential, relative minima current value, mean baseline current value, the polynomial coefficients of the regression, and the corresponding serotonin concentration. Once an electrode's data were processed for all serotonin standards of interest, a power law regression (Equation 12) was performed in Excel on the scatter plot of the repeated measures of current difference (mean  $\pm$  standard deviation) versus serotonin concentration.

$$y(x) = Ax^c \quad \text{Eq. 12}$$

A power law relationship allowed mapping from current value to concentration and vice versa.

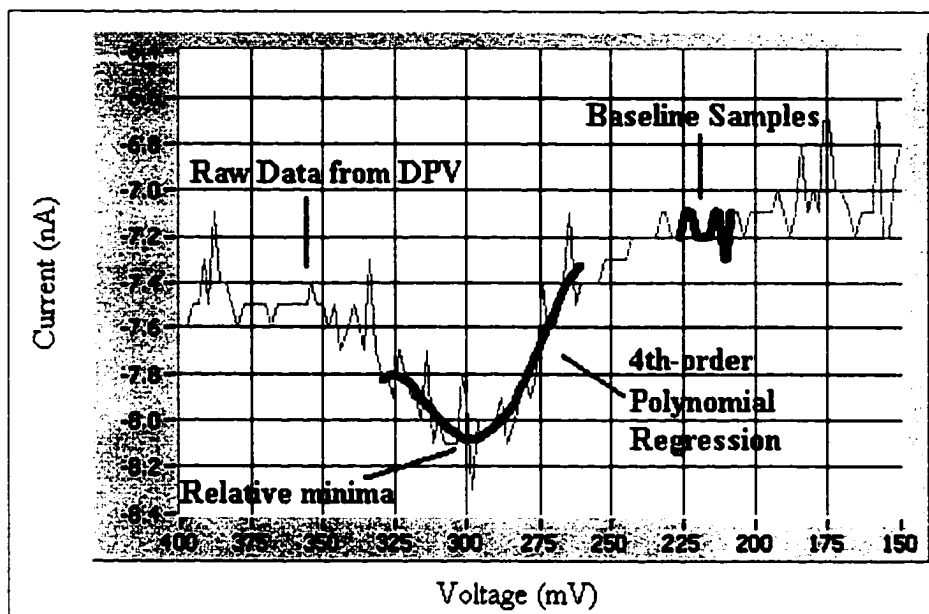


Figure 15 – Example of raw data analysis by Labview

## **2.4 Testing of Electrode in Blood**

### **2.4.1 Blood Collection and Processing**

Variants of blood were tested to establish electrode response to a biological environment. All blood used was from the same bovine source and was collected by animal-care professionals at the Louisiana Tech University farm. Experiments in this dissertation used whole blood, platelet-rich plasma (PRP), platelet-poor plasma (PPP), and dilute PRP. Whole blood was collected from the jugular vein into a 60 cc syringe (Cole Palmer) using a 16-gauge needle. Before blood collection, a 0.129 M sodium citrate solution (Sigma) was pre-loaded into the syringe to be used as the anticoagulant (ratio of blood to anticoagulant was 9:1). The needle was allowed to puncture the vein and blood was allowed to flow freely for three seconds before the syringe was connected to the needle. Once connected, the syringe barrel was slowly drawn back to the desired sample volume. Following blood collection, the needle was removed and the syringe

gently inverted four times to ensure proper mixing of the blood and anticoagulant. The syringe was kept at ambient temperature until experimental use or further processing. All experiments using whole blood were conducted within 30 minutes of blood collection. Protocols used for PRP and PPP generation were outlined in the clinical hematology text written by Corriveau and Fritsma<sup>53</sup>. PRP was created by placing the citrated whole blood in a centrifuge and spun at a force of 50 x g for 30 minutes at ambient temperature. After centrifugation, the PRP (top supernatant) was transferred into a sealed plastic vial with a sterile plastic pipette.

PPP was generated from the remaining supernatant by centrifuging at 2000 x g for 10 minutes at ambient temperature. Again, the PPP (top supernatant) was transferred into a sealed plastic vial with a sterile plastic pipette. Dilute PRP was created through the re-suspension of PRP with PBS. PRP was diluted with enough PBS to achieve the original blood volume present before centrifugation. For example, if 100 mL of citrated whole blood produced 10 mL of PRP, 90 mL of PBS was added to the PRP. All experiments conducted using PPP, PRP, or dilute PRP were conducted in fewer than 4 hours as recommended by Corriveau and Fritsma<sup>53</sup>.

#### **2.4.2 Uric Acid Interference Study**

This study was conducted to establish whether or not uric acid interfered with the detection of serotonin in PBS. Electrodes were calibrated with subsequent additions of serotonin as before, but the initial 5 mL of PBS medium contained a 200  $\mu\text{M}$  concentration of uric acid (Sigma). DPV was implemented to establish the potential at which 200  $\mu\text{M}$  uric acid is oxidized and corresponding change of baseline current. Following the electrode calibration with serotonin, 0.2 units of uricase enzyme (Sigma)

was added to the PBS/UA medium, and subsequent electrode measurements recorded the effect of uricase.

### **2.4.3 Serotonin Calibrations in Blood Variants**

Serotonin calibrations were conducted in whole blood, PPP/PRP, and dilute PRP with 0.2 units of uricase enzyme. Electrode sensitivity to serotonin and optimal medium for measurement was established through this experiment.

## **2.5 Static Study to Measure Serotonin Release from Platelets**

### **2.5.1 Preparation of Platelet Suspensions**

This study determined the effect that platelet-derived NO has on serotonin release due to activation by fibrillar collagen. Four different experimental situations were performed for this study (listed in Table 4). Dilute PRP was created in the same procedure as mentioned before from 100 mL of bovine blood. Experiments 1 and 3 serve as controls for experiments 2 and 4 respectively. Before experimentation, the 100 mL of dilute PRP was equally divided into two 50 mL aliquots, and treated with uricase enzyme (0.1 units per 5 mL of dilute PRP). Thirty milliliters of one aliquot were pre-treated for

**Table 4 – List of the four different experimental situations**

<b>Experiment #</b>	<b>Dish Surface</b>	<b>Medium</b>
<b>1</b>	Bare surface	PBS solution
<b>2</b>	Collagen surface	PBS solution
<b>3</b>	Bare surface	PBS solution with 1mM L-NMMA
<b>4</b>	Collagen surface	PBS solution with 1mM L-NMMA

five minutes before experimentation with 1 mM N<sup>G</sup>-methyl-L-arginine acetate salt (L-NMMA, Sigma). L-NMMA inhibits NO through competitive inhibition of all three

isoforms of NOS. Diluted platelet suspensions were used with four hours of PRP generation. Dishes were coated with fibrillar collagen on the night before the experiment.

### **2.5.2 Preparation of Fibrillar Collagen Film**

Twelve milliliters of chilled Vitrogen collagen (Cohesion Co., Inc.) was mixed with 1.5 mL of 10x phosphate buffered saline (Sigma) and 0.1 M NaOH. Solution pH was adjusted to  $7.4 \pm 0.2$  by the addition of a few drops of either 0.1 M HCl or 0.1 M NaOH. The final solution pH was verified with pH paper. Before use, the mixture (isotonic collagen solution) was stored in a refrigerator. To coat the surface of the tissue culture dishes, 1 mL of the isotonic collagen solution was added to dish surfaces. This volume covered the surface of the dish to a height of 1.5 to 2 mm. Each dish was then gently oscillated to ensure even distribution of the collagen solution throughout the surface of the dish. Then, each dish was covered and incubated for one hour at 37 degrees C to promote gelation. The dishes were then left uncovered in a laminar flow hood overnight or until dry. After drying, the collagen film was gently rinsed with distilled water to remove salts and to also rehydrate the film. Once complete, the film was used immediately or allowed to dry again for future use. After drying was achieved for the second time, unused dishes were refrigerated for future use.

Validation of the fibrillar collagen coating was achieved through staining with eosin. The collagen-coated dish was rehydrated with distilled water for 5 minutes. Next, the water was siphoned off and replaced with 10% buffered formalin solution for fixation. Following fixation, the dish was drained of formalin and rehydrated in water for 1 minute, 50% ethanol (ETOH) for 2 minutes, 70% ETOH for 2 minutes, 90% ETOH

with eosin for 1 minute, 95% ETOH for 1 minute, and 100 ETOH for 1 minute. Next, the dish was placed in the clearing agents, HistoClear II and HistoClear I, for 2 and 5 minutes respectively. The dish was immediately examined under a light microscope (Nikon) at a magnification of 100.

### **2.5.3 Serotonin Measurements in Dilute PRP**

The working and counter electrodes were electrically isolated and attached to each other with a mild adhesive in a parallel fashion with an average tip separation of 3 mm. A support arm of the micromanipulator held the electrode system at an angle of 30 degrees relative to the horizontal. The micromanipulator lowered the counter and working electrode system to a position above the dish surface (close to the surface, but not touching). Distance from dish surface to the electrode neck was approximately 1 mm. Another support arm secured the isolated reference electrode close to edge of the dish. Prior to DPV measurement, 5 mL of dilute PRP (with or without L-NMMA) was pipetted into the tissue culture dish. The physical setup described above was incorporated for both the coated and uncoated dishes and is illustrated in Figure 16.

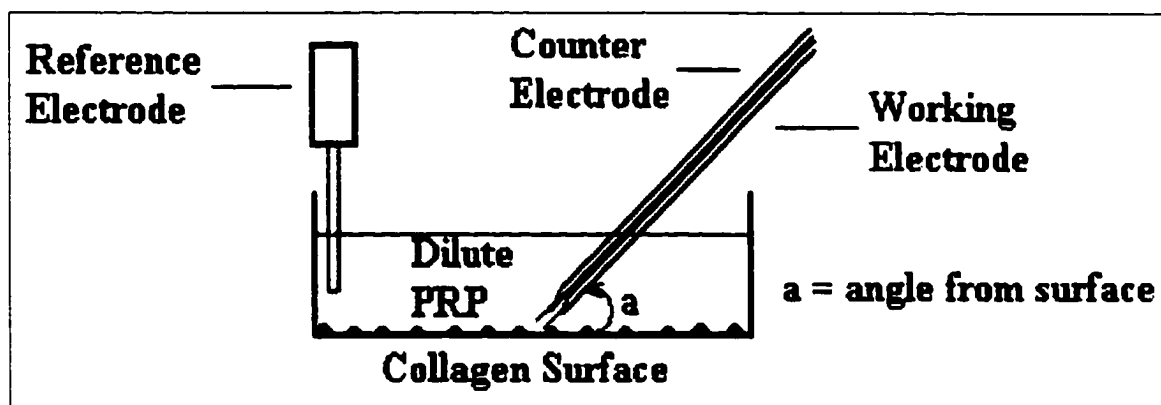


**Figure 16 – Physical setup for serotonin measurement from dilute PRP**

For each experimental situation, four replicates ( $N = 4$ ) were conducted with three repeated measures each. Fresh calibrated working electrodes were used for each replicate in the study. Analysis of DPV data was performed as described before and corresponding serotonin concentrations were quantified through each electrode's power law regression. At the completion of a replicate, the dish was promptly removed from the electrode system, drained of contents, gently rinsed with distilled water, and fixed with 10% buffered formalin. The dish was then set aside for future histological analysis.

#### **2.5.4 Histological Preparation and Analysis**

After electrochemical analysis, each tissue culture dish was fluorescently stained with acridine orange (Sigma). Acridine orange was mixed with distilled water to a final concentration of 0.1 g / 100 mL<sup>54</sup>. Procedure for acridine orange staining is as follows: the fixated tissue culture dishes were rehydrated in distilled water for 2 minutes and then rinsed in running distilled water for 5 minutes. Next, the dishes were stained in the acridine orange solution for 2 minutes and then rinsed in distilled water again for 30 seconds. Dishes were then dehydrated in 95 and 100 % ETOH for 1 and 3 minutes respectively. Clearing of excess stain was achieved through immersion in HistoClear II for 3 minutes. After staining, the dishes were covered, wrapped in foil to avoid exposure to light, and placed in a refrigerator until microscopic analysis could be performed. Acridine orange fluoresces with a mercury lamp using an excitation filter of 450 to 490 nm and a barrier filter of 520 nm<sup>55</sup>.

Each stained dish was examined under a light microscope with ultraviolet capabilities (Nikon) that was integrated with a digital camera (MS120, Kodak) connected to a Pentium PC running Photoshop 5.5 (Adobe) software. Images acquired from the

microscope system were imported into Photoshop and saved as high-quality JPEG image files. Five random locations in each dish were imaged at magnifications of 40, 100, and 400 in both the light and ultraviolet fields. A calibration slide, possessing a scale resolution of 10  $\mu\text{m}$ , was imaged in the light field at the different magnifications levels. Saved images of the calibration slide were used to accurately determine a length scale of the dish images.

Visual analyses of the resulting images from the static study were used to quantify platelet adherence. Ultraviolet images (from experiments 2 and 4) taken at magnifications of 40 and 100 were analyzed in Photoshop by counting the number of platelet aggregates adhered to the collagen surface. Analysis of the surface area covered by the platelet aggregates was performed with the following method. All images of interest were converted to grayscale. Through image processing capabilities within Photoshop software, a histogram of pixel brightness level was performed on each grayscale image. The range of brightness levels was from 0 to 255 with a bin resolution of unity. All image background levels were tested, and the threshold level for aggregate determination was set to 200. Measured value from the histogram was the number of pixels in the greater than or equal to a brightness level of 200. The ratio of measured value to total pixels present was a measure of percent surface area covered by platelet aggregates.

### **2.5.5 Statistical Procedures**

The change of current for each measurement performed with DPV was mapped back to a serotonin concentration using the electrode's power law regression to solve for the concentration level (Equation 13).  $A$  and  $C$  are regression coefficients,  $x$  is the

serotonin concentration in nM, and  $y$  is the measured current difference in nA. Statistics were performed on these calculated values of serotonin concentrations. Initially, a single-

$$x(y) = e^{\frac{\ln(y)}{c}} \quad \text{Eq.13}$$

factor analysis of variance (ANOVA) was performed using the different experimental procedures as treatment levels ( $\alpha = 0.05$ ). Tukey's test was performed for multiple comparisons across the four different treatment levels. For protection against an inflated error mean square, a two-factor ANOVA was also performed with the two factors defined as experiment type and replicate number ( $\alpha = 0.05$ ). Tukey's test was conducted for multiple comparisons between experiment types. Two-tail  $t$  tests ( $\alpha = 0.05$ ) were performed on the platelet aggregate counts and percent surface area data obtained from the Photoshop analysis.

## CHAPTER 3

### RESULTS

#### 3.1 Mathematical Modeling

##### 3.1.1 Agonist and Inhibitor Generation Model

Development of the agonist and inhibitor generation model assumed homogeneous species consumption in the plasma. TxA<sub>2</sub> is hydrolyzed to TxB<sub>2</sub> (thromboxane B<sub>2</sub>) by a first-order reaction, thrombin is inhibited by AT-III through a second-order reaction, and NO is also consumed through a second-order reaction with superoxide. Although the reactions involving NO and thrombin are second-order kinetics, pseudo first-order reaction rates may be calculated if plasma concentrations of AT-III and O<sub>2</sub><sup>-</sup> are assumed to be constant,<sup>24</sup>. Plasma concentrations of AT-III and O<sub>2</sub><sup>-</sup> were assumed to be 4 μM and 0.6 nM respectively. Table 5 shows the model parameters for TxA<sub>2</sub>, thrombin, and NO transport with calculated surface flux and first order

**Table 5 – Parameters for agonist and inhibitor generation model**

Species	D <sub>AB</sub> (cm <sup>2</sup> /s)	K (surface flux)	Inhibitor	k (reaction)
TxA <sub>2</sub>	2.14 x 10 <sup>-6</sup>	2.3 x 10 <sup>-7</sup> μmol/(cm <sup>2</sup> -s)	Hydrolysis	0.0161 s <sup>-1</sup>
Thrombin	4.16 x 10 <sup>-7</sup>	1.5 x 10 <sup>-10</sup> unit/(μm <sup>2</sup> -s)	AT-III	0.0283 s <sup>-1</sup>
NO	3.30 x 10 <sup>-5</sup>	5.94 x 10 <sup>-8</sup> μmol/(cm <sup>2</sup> -s)	O <sub>2</sub> <sup>-</sup>	4.02 s <sup>-1</sup>

constants (k). Figures 17 through 19 illustrate the concentration profiles of TxA<sub>2</sub>, reaction thrombin, and NO respectively. The plots are shown on a semi-logarithmic

graph with multiple curves super-imposed on the same graph. Each curve represents a different time during the transient analysis of concentration as a function of axial position from the collagen surface. Proceeding in a bottom-to-top fashion, the curves represent times of 0.1, 0.25, 0.5, 1, 5, and 60 seconds respectively.

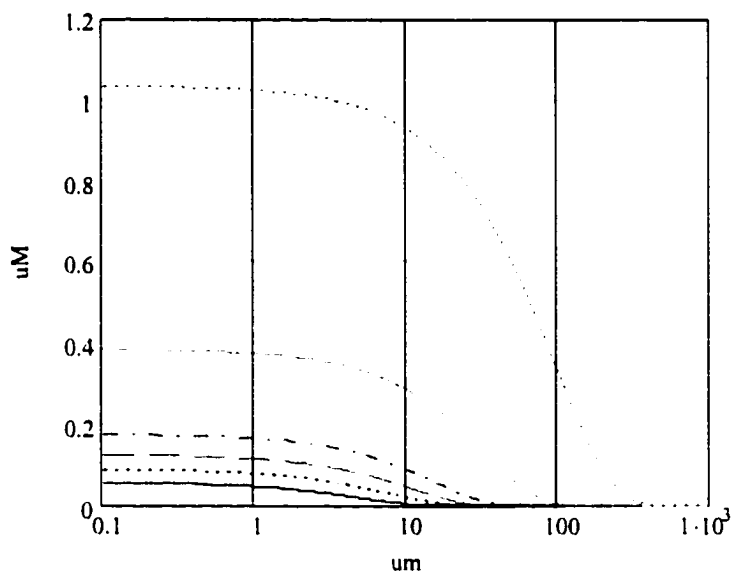


**Figure 17 – TxA2 transport**

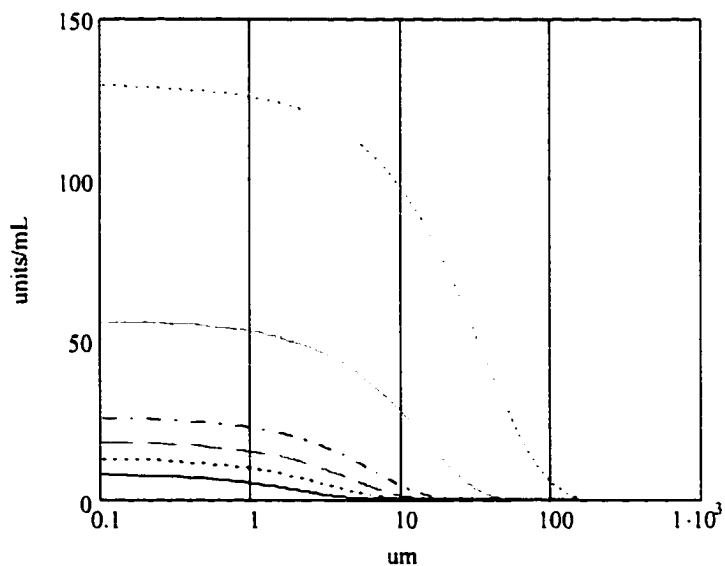


**Figure 18 – Thrombin transport**

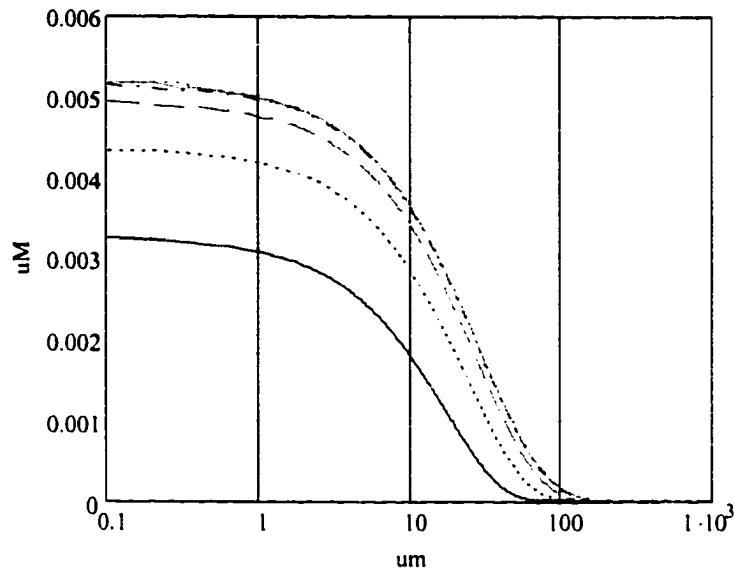


**Figure 19 – NO transport**

From inspection of the three plots, high concentrations of TxA2, thrombin, and NO are isolated to within the first 10  $\mu\text{m}$  of platelet aggregation. Similar shapes of the concentration profiles were expected since the same model was used for all three cases; however, each species transport characteristics are different due to individual diffusion coefficients and reaction kinetics. Due to the assumption of a constant surface flux for all time, these models represent upper bounds for agonist and inhibitor concentrations, thus creating a worse-case scenario with respect to coagulation. Since consumption exists in the plasma, steady-state concentration profiles are bounded. The time to reach steady state for TxA2, thrombin, and NO under the modeling assumptions were calculated to be 500, 285, and 2 seconds respectively. Steady-state concentration profiles were normalized for each of the species and plotted in figure 20. Proceeding from left to right, the profiles correspond to NO, thrombin, and TxA2.

The model demonstrates that maximal levels of platelet-generated NO are reached very quickly (within 2 seconds) at the platelet surface, possibly playing a role in the local

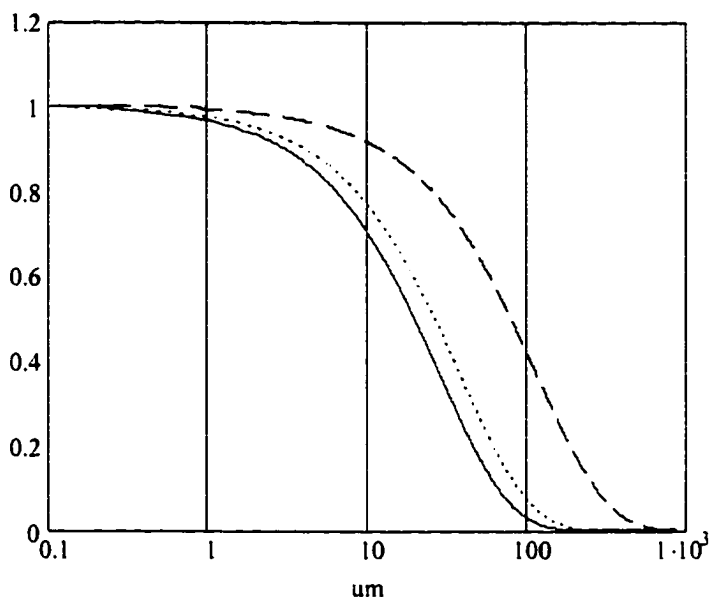


**Figure 20 – Normalized steady-state concentration profiles of TxA2, thrombin, and NO**

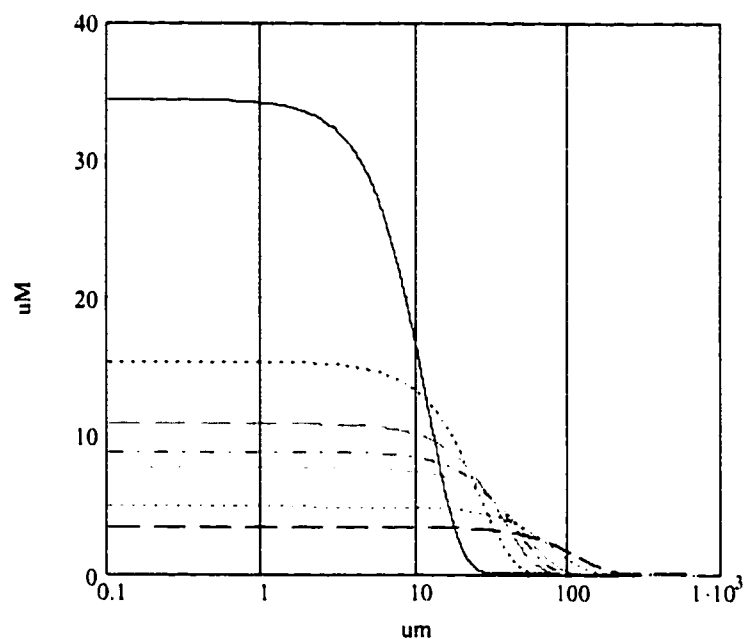
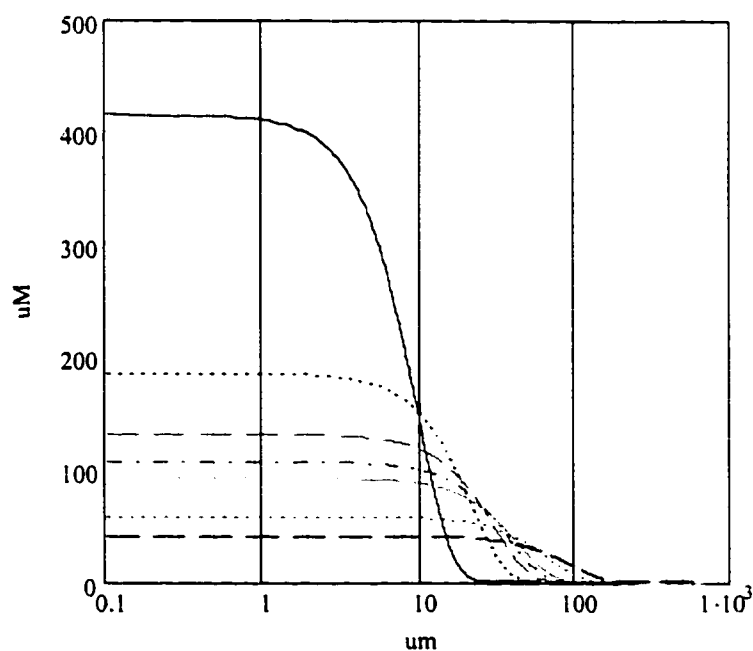
suppression of coagulation. However, as time progresses on the order of minutes, increasing levels of TxA2 and thrombin begin to reach their maximum concentrations thereby increasing the spatial extent of agonists at critical concentrations.

### **3.1.2 Agonist Release Model**

The parameters used as constants for the serotonin and ADP transport models are listed in table 6. It is assumed that platelets are uniformly distributed across the collagen surface in a monolayer fashion and that their granular contents are expelled instantly upon activation by collagen. The value  $m_0$  represents the amount of agonist released from the adhered platelets per square surface area. Figures 21 and 22 illustrate the concentration profiles of serotonin and ADP transport respectively. The plots are shown super-imposed on the same graph. Each curve represents a different time during the transient analysis of concentration as a function of axial position. Proceeding in a top-to-bottom manner, the curves represent times of 0.1, 0.5, 1.0, 1.5, 2.0, 5.0, and 10.0 seconds

**Table 6 – Model parameters for agonist release model**

Species	$D_{AB}$ (cm <sup>2</sup> /s)	Amount per platelet	$m_0$ (calculated)
Serotonin	$3.45 \times 10^{-6}$	$0.3 \times 10^{-11}$ $\mu$ mol	$7.16 \times 10^{-13}$ $\mu$ mol/ $\mu$ m <sup>2</sup>
ADP	$2.57 \times 10^{-6}$	$3.0 \times 10^{-11}$ $\mu$ mol	$7.16 \times 10^{-12}$ $\mu$ mol/ $\mu$ m <sup>2</sup>

**Figure 21 – Serotonin transport****Figure 22 – ADP transport**

respectively.

Since serotonin and ADP are released and not continuously generated, surface concentrations do not increase with time. These species are not homogeneously consumed in the plasma, but the concentration profiles decrease in an exponential manner with distance from the adhered platelets. Concentration profiles asymptotically approach zero as distance increases to infinity. As shown in the figures representing ADP and serotonin transport, sub-micromolar concentrations are achieved before 100 microns. According to the model, maximum agonist concentrations are found at the surface of adhered platelets. As time increases, these surface concentrations also decay in an exponential fashion. More specifically, serotonin and ADP surface concentrations are 75% of their initial maximum value at 2 and 0.18 seconds respectively. Fifty percent is achieved at 4 and 0.4 seconds, 25% at 16 and 1.62 seconds, and 5% at 400 and 40 seconds respectively. Although the diffusion coefficients for serotonin and ADP are on the same order of magnitude, differences in their concentration profiles are attributed to amount of agonist release per platelet. The molar amount of dense granule serotonin is ten times less than dense granule ADP concentration. *In vivo*, it is possible for increased ADP concentrations due to erythrocyte ADP liberation<sup>32</sup>. Results of the release model for serotonin give support to the hypothesis that local serotonin concentrations are too low in magnitude for platelet activation, and it may act to potentiate ADP and thrombin activation<sup>27</sup>.

### **3.2 Serotonin Sensor Development**

The electrode fabrication process yielded excellent results with respect to cost, production rate, and reproducibility. Ease of construction allowed fresh electrodes for each experiment performed. The rate-limiting step during the entire fabrication process was the overnight tip immersion in NaOH to remove excess beeswax, which took an average of eight hours to complete. Before saponification, it is possible to fabricate twenty-five electrodes within an hour. Initial starting costs are moderately high due to the purchase of medical grade carbon fibers; however, several thousand electrodes can be made from the purchased spool. Additional hardware costs such as copper wire, beeswax, silver epoxy, and glass capillaries are minimal.

Through empirical observation, electrodes stored dry in a dust-free environment possessed a longer shelf life than those stored immersed in distilled water. When stored in water for a long period of time, reduced sensitivity is observed, perhaps due to microbial growth fouling the sensor's carbon surface. Before calibration, microscopic analysis in the light field was performed to ensure proper tip sealing with beeswax, verify the proper number of fibers comprising the tip, scan the electrode shank for any cracks within the glass capillary, and ensure continuity between the carbon fiber and copper conductor. Figures 23 through 25 show the various parts of a typical sensor developed for this research project.

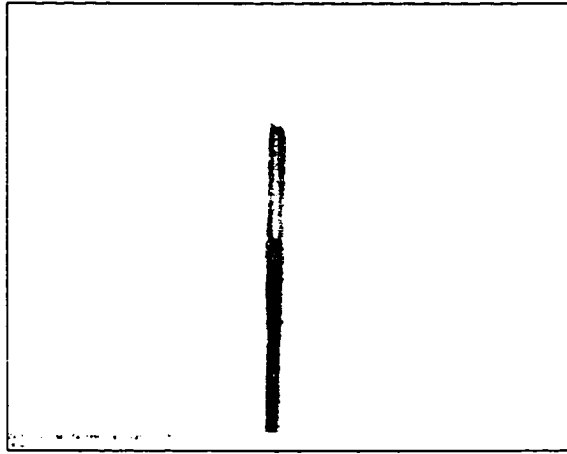


**Figure 23 – Carbon fiber tip of sensor made of two fibers (100x)**

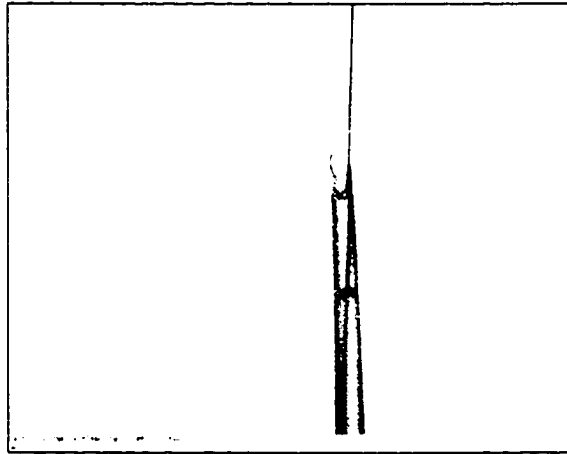


**Figure 24 – Sealed neck of sensor with protruding fiber (40x)**

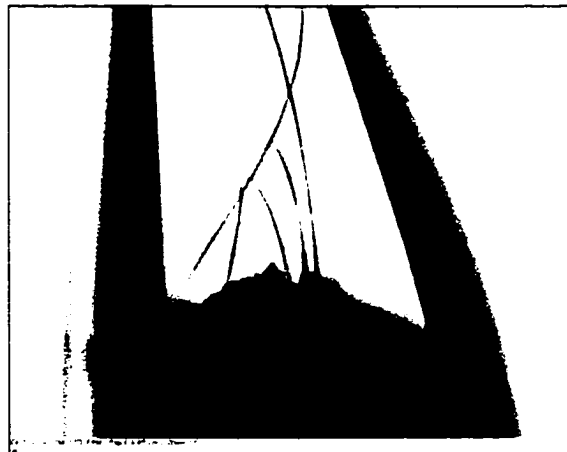


**Figure 25 – Interface of carbon fibers with copper conductor (40x)**

### **3.3 Sensor Calibration**

#### **3.3.1 Sensor Detection Limits**

Calibration range for the serotonin sensor was based on the detection limits observed in the laboratory. In the literature, it was reported that carbon fiber electrodes using DPV could achieve detection limits in the nanomolar range (parts per billion). Of course this value is dependent upon electrode size and electrochemical properties of the species of interest. Therefore a simple test was performed to establish a lower detection limit for the probe. A serotonin standard was made so that injection of one aliquot in an electrochemical cell with PBS produced a final concentration of 1 nM. DPV scans were performed for each aliquot added, and it was discovered, on average, that a concentration of 4 nM was the smallest detectable amount of serotonin that could be distinguished from the background Gaussian noise of the current signal. Figure 26 illustrates a current deflection caused by a 4 and 144 nM serotonin standard.

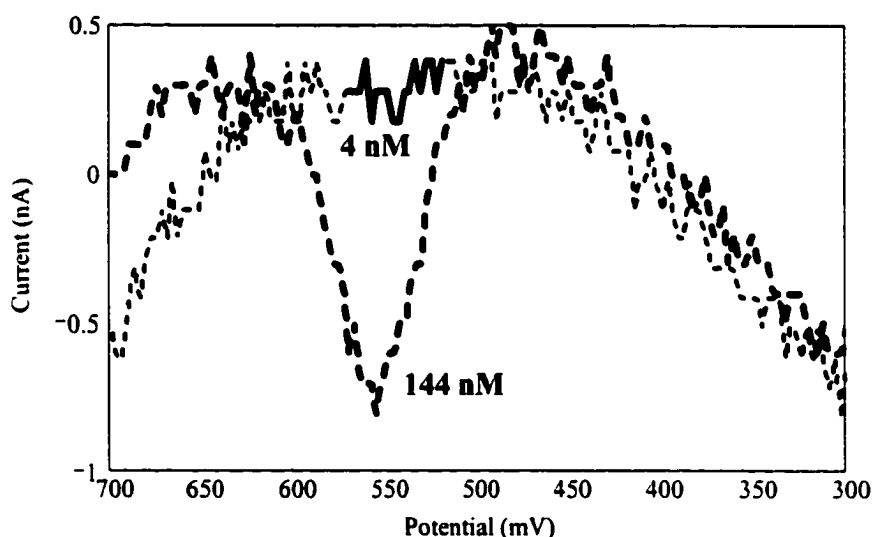


**Figure 26 – Deflections in DPV scans corresponding to 4 and 144 nM serotonin**

The region around 550 mV represents the change in baseline due to the oxidation of both serotonin levels on the carbon surface. Actual oxidation potential of serotonin is probe dependent; however, it was observed to always be in range of  $550 \pm 50$  mV. This potential is within the range published in the literature. For example, Bull *et al.* found the oxidation potential for serotonin to take place at 579 mV<sup>56</sup>. It appears that the current produced from the 4 nM standard is larger than the 100 pA noise magnitude. Any probe that failed to detect the 4 nM serotonin control during the calibration process was discarded.

A detection limit for the maximal amount of serotonin was also found. In theory, it is usually assumed that the analyte concentration at the probe's catalytic surface is zero due to immediate species oxidation. This assumption is valid for low concentration levels, but at elevated concentrations, the flux of analyte to the sensing element occurs faster than the oxidation reaction. Therefore, analyte begins to accumulate on the tip resulting in a plateau of current despite increased concentrations. To find the upper boundary for serotonin detection, additional serotonin aliquots were administered to the cell until no change in current was detected when compared with the previous scan. It was found that the maximum detectable limit of serotonin concentration on average was 300 nM. Figure 27 illustrates a scatter plot of typical sensor calibration data. After 300 nM there is a slight decrease in current value, indicating an upper bound detection limit.

### **3.3.2 Power Law Regression of Calibration Data**

Upon completion of probe calibrations and data processing in Labview, scatter plots of current versus serotonin concentration (mean  $\pm$  stdev) were generated in Excel. At first glance, the calibration data followed a linear trend with a high degree of

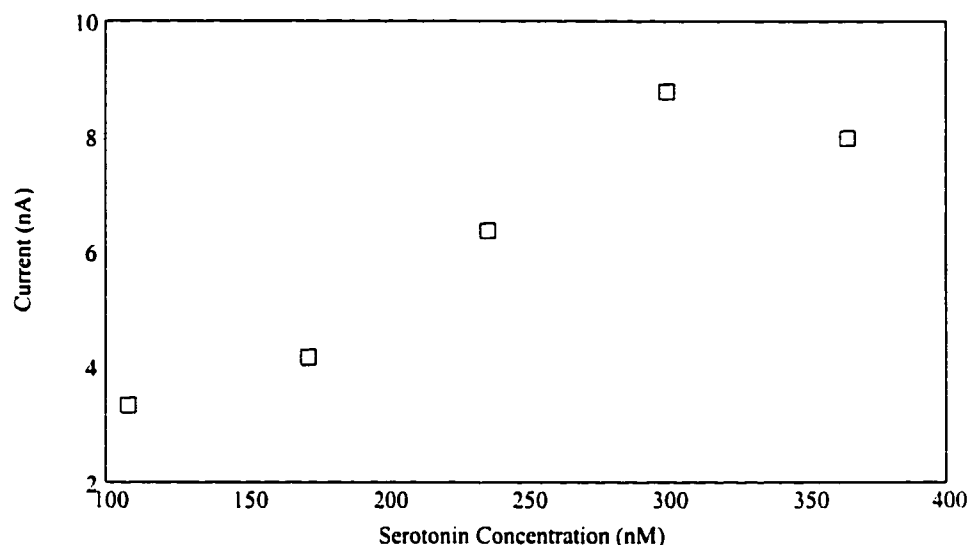


**Figure 27 – Example upper saturation limit from calibration**

correlation. However, closer inspection of the plot showed that the linear trend was only isolated only to the high concentration values with excellent agreement. The regions of low concentration revealed nonlinear trends. When the regressional analysis was performed using a power law regression, good agreement with a high degree of correlation was achieved in both the low and high concentration values. Therefore, power law regression was used to mathematically model the electrode's calibration data. Figure 28 shows a typical calibration curve for serotonin, and Table 7 compares the correlation ( $R^2$ ) differences between a linear and power law regression for the calibration data of seven independent electrodes.

It is also proper to note here that the standard deviations of the repeated measures increased with increasing serotonin concentrations (as seen in Figure 28). On average, minimal variance within the electrode calibrations was seen at the minimal detection limit of 4 nM. As serotonin concentration approached the upper detection limit, variance

increased. This upper limit is believed to be attributed to the current plateau caused by the accumulation of serotonin at the electrode's surface.

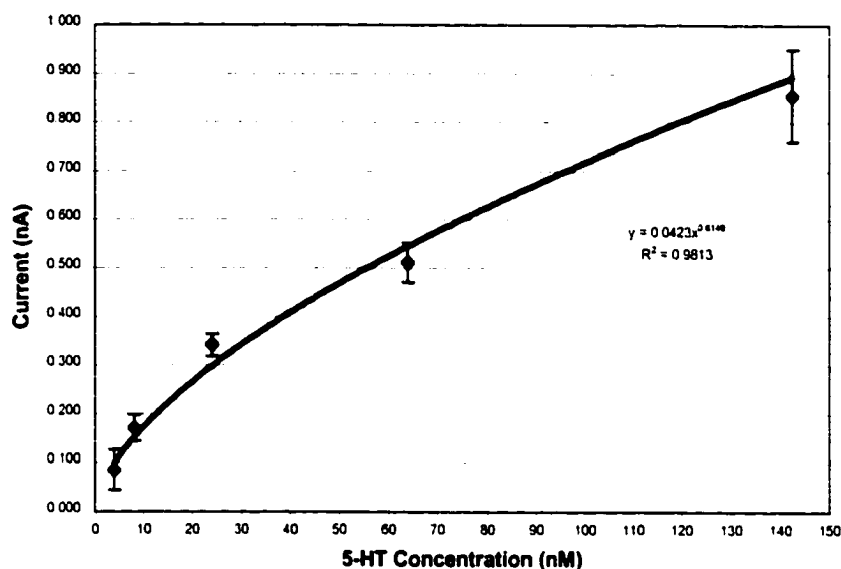


**Figure 28 – Example of power law for an electrode calibration**

**Table 7 – Comparison between linear and power law correlation values**

Electrode	Linear	Power
BR8	0.9785	0.9821
BR9	0.9849	0.9999
BR6	0.9415	0.9874
BE4	0.8531	0.9049
BE8	0.7899	0.8760
BE9	0.9858	0.9939

### **3.4 Testing of Electrode in Blood**

#### **3.4.1 Uric Acid Interference**

Since all electrodes were calibrated in PBS, interfering species were not present.

When an attempt was made to interface the electrodes in bovine blood to achieve a baseline DPV, the effects of interfering species became present. An analysis and

literature search determined what was interfering electrochemically with the electrode at a similar potential as serotonin. Table 8 depicts possible interfering species that are electrochemically active and present in the plasma. Uric acid proved to be a viable candidate due its large concentration in mammalian plasma.

Testing was performed with 200  $\mu\text{M}$  uric acid dissolved in PBS, and upon conclusion of the baseline DPV scan; UA was oxidizing at average potential of  $544 \pm 5$  mV. This potential was almost exactly the same as the potential for serotonin. Since DPV requires at least a 50 mV potential to discriminate between multiple species, UA was eliminated through the use of the enzyme uricase. Uricase is an enzyme that converts UA to allantoin, which is electrochemically inert<sup>57</sup>. When a final PBS solution containing 150  $\mu\text{M}$  UA and 200 nM serotonin was created, the serotonin signal could not be differentiated from UA. Upon addition of 0.2 units of uricase, UA interference was suppressed and the signal due to serotonin was resolved. This result implied that uricase does not interfere with serotonin measurements.

It was observed that UA returns a higher current value than serotonin at physiological concentration. For example, a 200 nM serotonin concentration would cause a 5 nA deflection from baseline, whereas a 150  $\mu\text{M}$  UA would cause a 70 nA deflection. Since each molecule is similar in formula weight, differences must arise in the oxidation reaction.

### **3.4.2 Testing in Blood Variants**

With uricase to inhibit UA, blood variants consisting of whole blood, PPP, and dilute PRP were tested with known quantities of serotonin. When increased amounts of serotonin were added to whole blood and PPP, change in current due to serotonin

**Table 8 – Possible interferences: the means and expected ranges of readily oxidizable, secretory products in adult human plasma**

<u>BIOCHEMICAL</u>	<u>MEAN</u>	<u>RANGE</u>	<u>PAGE*</u>
Glucose	5.52mM	4.55-6.50 mM	605
Glutathion	925. $\mu$ M	703-1082 $\mu$ M	573 (only in erythrocytes)
Urate	289. $\mu$ M	124-454 $\mu$ M	577
Glutamate	58.5 $\mu$ M	17-118 $\mu$ M	574
Tyrosine	50.2 $\mu$ M	35.9-62.3 $\mu$ M	574
Tryptophan	48.0 $\mu$ M	25.0-73.0 $\mu$ M	574
Cysteine	41.7 $\mu$ M	27.1-79.4 $\mu$ M	574
Ascorbate	27.0 $\mu$ M	11.1-49.7 $\mu$ M	611
Nitrite	174. nM	0-348 nM	564 (whole blood)
Acetylcholine	87.6 nM	0-252 nM	575
Serotonin	73.8 nM	5.7-142 nM	575
Dopamine	9.6 nM	$\pm$ 2.9 nM	733
Norepinephrine	1.8 nM	$\pm$ 0.4 nM	733
Epinephrine	0.33nM	$\pm$ 0.28 nM	733
Peroxide	~ pM		
Sup eroxide	~ pM		

\*Geigy Scientific Tables 7ed., K. Diem, C. Lentner eds., Ciba-Geigy Ltd. Basle, Swit. (1970)

oxidation was not seen. Instead, poisoning of the electrode was observed. Since the tip is held at positive potentials and most of blood colloidal species of the blood and plasma are negatively charged, it is possible that the electrode tip became contaminated with blood proteins creating a diffusion barrier to serotonin. The dilute PRP has the same platelet concentration as whole blood, but about one-tenth the protein content. Signals due to serotonin oxidation were observed during calibration with dilute PRP. Scatter plots were similar to the ones obtained from calibration in PBS. Therefore, it was concluded that serotonin measurements could be made in dilute PRP without interference due to sensor fouling.

### **3.5 Static Study to Measure Serotonin Release from Platelets**

#### **3.5.1 Evaluation of Fibrillar Collagen Film**

The fibrillar collagen coating of the tissue culture dishes was the sole activator of platelet activity in the static study. It is known that platelets are activated by and adhere to fibrillar collagen. Therefore, it was pertinent to determine histologically if the collagen surface was fibrillar or not. Figure 29 is a collagen image taken from a tissue culture dish prepared with fibrillar collagen as outlined in the methods section. Collagen stains pink when eosin is used as the staining agent, and fibrillar formations are easily seen in the background of the image. This image was compared with a microscopic illustration of collagen provided in a histology laboratory manual, and the microscopic features matched.

### **3.5.2 Measurements in Dilute PRP**

For each trial performed (four in all), a fresh electrode was used. Data obtained from the electrodes was mapped back to a serotonin concentration through the use of



**Figure 29 – Fibrillar collagen coating in tissue culture dish (100x)**

Equation 13. Regression constants, A and C, are specific for each electrode used. Table 9 below presents the serotonin concentrations as a function trial number and experiment type. From inspection of the concentration values listed in Table 9, many of the values are below the 4 nM detection limit for serotonin. These values are considered to be in the noise region of the sensor and they represent current levels that are below 100 pA. Since the background noise is Gaussian and random in nature, it is present in all measurements made from the sensor. If these values below 4 nM were forced to take on a value of zero, the average magnitude of the random noise would have to be subtracted from the remaining measurements as well. Keeping the sub-threshold values does not violate that statistical analysis.

**Table 9 – Serotonin data from static study in dilute PRP**

	Exp 1 (nM)	Exp 2 (nM)	Exp 3 (nM)	Exp 4 (nM)
<b>Trial 1</b>	1.77	10.10	6.24	17.18
	3.15	19.65	3.96	48.82
	3.00	17.12	0.68	12.51
<b>Trial 2</b>	8.51	19.66	1.15	14.72
	5.07	14.96	0.38	7.81
	5.07	13.93	2.52	3.76
<b>Trial 3</b>	2.86	16.57	0.49	3.86
	0.51	24.87	2.17	14.49
	1.56	17.50	2.82	16.93
<b>Trial 4</b>	1.95	5.13	3.52	11.91
	1.86	9.25	1.50	6.92
	1.31	4.07	1.17	8.35

**3.5.2.1 Single Factor ANOVA.** Initially a single factor ANOVA was performed on the data with experiment type designated as the treatment levels. Thus, four treatments are present. The different treatments/experiments are: (1) no collagen with dilute PRP (2) collagen with dilute PRP (3) no collagen with dilute PRP and L-NMMA and (4) collagen with dilute PRP and L-NMMA. The single factor ANOVA will indicate if any of the means are statistically different. If so, a multiple comparison test will show the treatment levels that are statistically different. Tukey's multiple comparison test was chosen because it has a type I error rate of  $\alpha$  for all pair wise comparisons on an experiment wise basis<sup>58</sup>. Table 10 shows the single factor ANOVA results. The ANOVA indicates that the treatment means are statistically different with a  $P < 0.0001$ .

In performing the Tukey test, the test statistic ( $T$ ) was calculated by equation 14.

$$T = q_{\alpha}(a, f)S_{y_i} \quad \text{Eq. 14}$$

Where  $q_{\alpha}(a, f)$  is the studentized range statistic with  $a$  treatments and  $f$  is the number of

**Table 10 – ANOVA table for single factor experiment with four treatment levels**

ANOVA: Single Factor

## SUMMARY

<i>Groups</i>	<i>Count</i>	<i>Sum</i>	<i>Average</i>	<i>Variance</i>
Exp1	12	36.617	3.051	4.904
Exp2	12	172.815	14.401	38.57
Exp3	12	26.600	2.216	2.989
Exp4	12	167.264	13.938	142.387

## ANOVA

<i>Source of Variation</i>	<i>SS</i>	<i>df</i>	<i>MS</i>	<i>F</i>	<i>P-value</i>	<i>F crit</i>
Between Groups	1602.393	3	534.131	11.312	1.26E-05	2.816
Within Groups	2077.422	44	47.214			
Total	3679.815	47				

degrees of freedom for error.  $S_{y_i}$  is the standard error for each average calculated by Equation 15.

$$S_{y_i} = \sqrt{\frac{MS_E}{n}} \quad \text{Eq. 15}$$

$T$  is calculated to be 7.518, implying that two means are significantly different if the absolute value of their sample differences exceeds this value. From inspection of the sample means based on treatment levels, comparisons of experiments 1 to 2, 2 to 3, 1 to 4, and 3 to 4 show statistical differences.

From this single factor analysis it can be concluded that serotonin concentrations are elevated in the presence of fibrillar collagen when compared with the absence of collagen. Presence of the NOS inhibitor, L-NMMA, did not have a statistical significance when compared across experiments with fibrillar collagen, which lacked L-NMMA. It can be inferred from this analysis that a statistically significant change in

serotonin concentration, resulting from platelet activation by collagen, could not be detected when compared in presence and absence of the NOS inhibitor L-NMMA.

**3.5.2.2 Two-Factor ANOVA.** Since each experiment was composed of four independent trials with three repeated measures each, a two-factor ANOVA was run to guard against an inflated error mean square. The two factors were experiment type and trial. Another advantage to this analysis was performance of an interaction analysis between experiment type and trial. When a comparison is made between the single and two factor ANOVA tables, the error mean square was reduced from 47.2 to 34.7, which is a 26.5% reduction. The results are similar to the single factor ANOVA since the treatment means are still experimentally different with a  $P < 0.0001$ . Table 11 shows the obtained results. Information is now

**Table 11 – Two-factor ANOVA results (factors are experiment and trial)**

Two-factor ANOVA						
<i>Source of Variation</i>	<i>SS</i>	<i>df</i>	<i>MS</i>	<i>F</i>	<i>P-value</i>	<i>F crit</i>
Trial	319.254	3	106.418	3.064	0.042	2.901
Experiment	1602.393	3	534.131	15.378	2.268E-06	2.901
Interaction	646.685	9	71.854	2.069	0.063	2.188
Within	1111.482	32	34.734			
Total	3679.815	47				

obtained about the local repeated measures as well as interaction between trials and treatment types. Figure 30 is a plot of the interaction between trials and experiment types. This interaction is marginally significant ( $P = 0.063$  in table 11).

Tukey test was again used to compare among experiment means over trials. For this multiple comparison analysis, a T value of 13.00 was calculated. Statistical differences were shown for trial 1 between experiments 1 and 2, 1 and 4, and finally

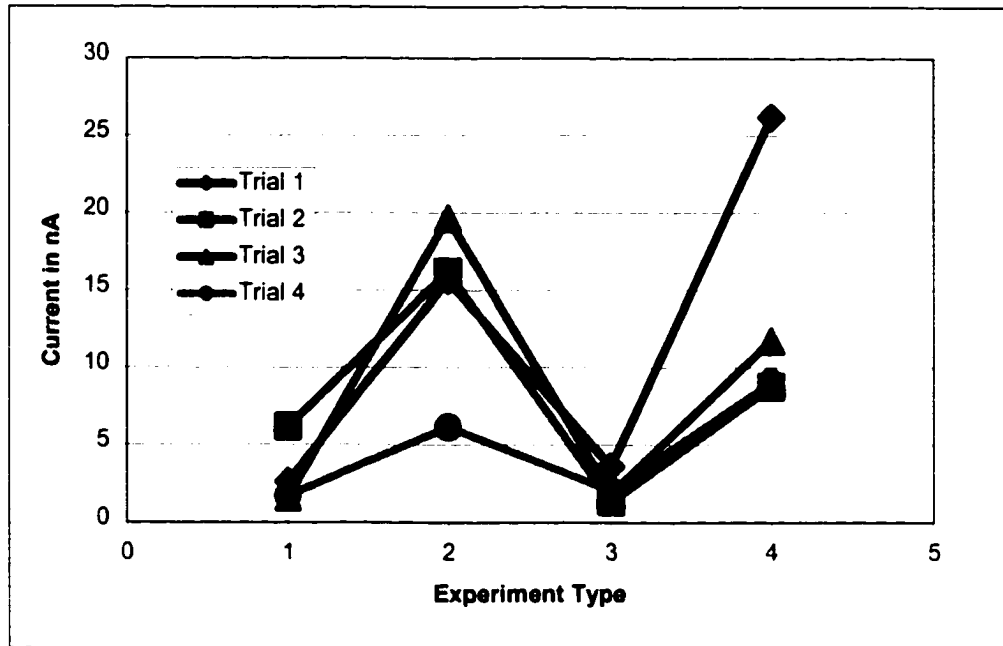


**Figure 30 – Interaction analysis for the two-factor ANOVA**

3 and 4. For trial 2, differences were shown only for experiments 2 and 3. For trial 3, differences were shown for experiments 1 and 2, followed by experiments 2 and 3. In trial 4, no differences between experimental means were observed. Some interaction does occur across the trials performed for each experiment; however, as seen below conclusions drawn about the marginal effects across the different experimental parameters remain the same as those drawn from the single factor ANOVA. It is possible that interaction between trials and experiment type is a result of tip fouling from the three repeated measures taken consecutively.

A final comparison between experiment types was conducted using the marginal means of experiment type. This comparison was performed to see if the same conclusion could be drawn about the experiment as in the single factor ANOVA. Tukey test was again used and a T value of 6.50 was calculated. Statistical differences were observed for experiment groups 1 and 2, 1 and 4, 2 and 3, and finally 3 and 4. These results exactly

match those of the single factor ANOVA, however the two-factor ANOVA had a reduced the error mean square value by 26.5 percent.

### **3.5.3 Histological Analysis of Adhered Platelets**

Initial verification of adhered platelets was performed by finding an aggregate at a magnification of 400 in the UV field, followed by scale measurements of the same aggregate in the light field. A magnification of 400 proved to be sufficient resolution to measure individual particle sizes of the resulting aggregate. Since platelets have an average diameter of 2 to 3 microns, a magnification of 400 is powerful enough to resolve individual platelets. Figure 31 represents the morphology and composition of a typical



**Figure 31 – A typical aggregate showing individual platelets with a 10  $\mu\text{m}$  scale (400x)**

platelet aggregate at 400x. The aggregate shown in figure 30 is irregular in shape and has a width and height of approximately 30  $\mu\text{m}$  and is typical of thrombus size reported in the literature <sup>59</sup>. A scale superimposed on the figure has divisions of 10  $\mu\text{m}$ . Individual

platelets can be resolved and they appear as small, light-colored areas scattered across the thrombus surface.

Tissue culture dishes were randomly chosen from the four experimental conditions. Each dish was fixated with formalin and stained with acridine orange as described before. Acridine orange was chosen as the fluorescent stain since it is selective to platelet cytoplasm, thus, allowing the entire aggregation of platelets to fluoresce under ultraviolet light. When dishes from experiments 1 and 3 were observed in both the light and UV fields, platelet aggregates were not present. Examination of dishes from experiments 2 and 4 revealed platelets aggregates adhered to the collagen surface scattered throughout the dishes. Figures 32 and 33 represent microscopic images of

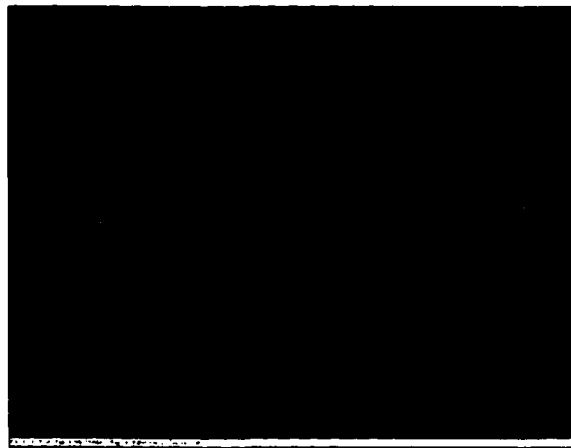


**Figure 32 – Adhered platelet aggregates on collagen (40x from experiment 2)**  
platelet aggregates at a magnification of 40 in the UV field for experiments 2 and 4 respectively.

Five independent random measures for each dish were obtained for the number of aggregates and percent surface coverage of the 40x and 100x field. Experimental data for the five random measures is presented in Tables 12 and 13 below.



**Figure 33 – Adhered platelet aggregates on collagen (40x from experiment 4)**

**Table 12 – Data from platelet count on collagen surface for 40x and 100x (N = 5)**

<b>Count of Platelet Aggregates on Collagen Surface</b>				
<b>Measure Number</b>	<b>40x Field</b>		<b>100x Field</b>	
	<b>Exp 2</b>	<b>Exp 4</b>	<b>Exp 2</b>	<b>Exp 4</b>
<b>1</b>	50	36	7	10
<b>2</b>	42	38	13	6
<b>3</b>	34	34	12	19
<b>4</b>	40	49	10	11
<b>5</b>	40	47	8	8
<b>P = 0.92</b>			<b>P = 0.74</b>	

Results of the two-tail t-tests performed between experiments 2 and 4 for magnifications of 40 ( $P = 0.92$ ) and 100 ( $P = 0.74$ ) showed no statistical significance for the number of adhered platelet aggregates. Examination of the total surface area covered by platelet aggregates was also found to be insignificant when compared at magnifications of 40 ( $P = 0.10$ ) and 100 ( $P = 0.66$ ). The magnitudes of aggregate number and size appear to be independent of NOS inhibition. Results from histological analysis support the conclusions obtained from the electrochemical measurement of serotonin.

**Table 13 – Data from percent surface area coverage by platelets on collagen surface for 40x and 100x (N = 5)**

<b>% Surface Area Occupied by Platelet Aggregates on Collagen Surface</b>				
<b>Measure Number</b>	<b>40x Field</b>		<b>100x Field</b>	
	<b>Exp 2</b>	<b>Exp 4</b>	<b>Exp 2</b>	<b>Exp 4</b>
<b>1</b>	3.47	2.19	2.41	3.52
<b>2</b>	1.96	1.96	5.38	2.20
<b>3</b>	2.12	1.96	3.31	4.80
<b>4</b>	2.55	1.90	3.40	3.23
<b>5</b>	2.29	1.93	3.16	1.95
	P = 0.10		P = 0.66	

## **CHAPTER 4**

### **DISCUSSION**

#### **4.1 Mathematical Models**

Serotonin, released from platelet dense granules upon activation, is believed to be influenced by platelet-derived NO. Due to the short half-life of NO observed at physiological levels, direct measurement of NO in real-time is non-trivial. Therefore, it was hypothesized that platelet-derived NO may modulate the release of platelet granule contents. Due to its stability and favorable electrochemical properties, serotonin was chosen as the species for direct measurement. Experiments performed in this dissertation were designed ultimately to measure serotonin directly in dilute plasma in the presence and absence of the NOS inhibitor L-NMMA. Preliminary modeling of platelet agonists and inhibitors, through static diffusion simulations, provided insight about the transport characteristics and surface concentrations of serotonin, NO, TxA<sub>2</sub>, and thrombin. Knowing the surface concentrations and chemical kinetics resulting from thrombus formation is critical in understanding atherosclerosis. Mathematical models supported by electrochemical measurements are only validated through direct histological evidence of platelet adherence.

The mathematical models represent upper bounds on platelet-derived agonist and inhibitor concentrations. Assumptions made before model development allowed for

analytical solutions to be obtained, but modeling of the more complicated conditions found *in vivo* and *in vitro* would require numerical solutions. For example, ADP and serotonin release from platelets occurs over an extended time as the platelets adhere and form aggregates. The model assumes granule release happens instantly from the entire thrombus, but this type of release does not occur *in vivo* or *in vitro*. Inspection of adhered platelets on collagen in this study supports the idea that thrombus formation is a diffuse process and does not progress uniformly even when highly thrombogenic surfaces such as collagen are exposed during experimentation. Although the models developed for this project are idealized cases, pertinent information with respect to the transient development of critical agonist and inhibitor surface concentrations was ascertained. These models assumed a uniform platelet distribution across the entire collagen surface. It was not desired to predict the time course of or platelet adhesion and aggregation processes, due to complex interactions between agonists and inhibitors<sup>24,25</sup>.

Generation of platelet-derived agonists and inhibitors is assumed to progress in a constant fashion, only hindered by homogeneous reactions in the plasma. Reactions in the simulation are assumed to depend only upon concentration of the species modeled via first-order kinetics. For example,  $O_2^-$  concentration is relatively constant in the body, but it may be variable in close proximity to a platelet thrombus. NO is believed to be the rate limiting species in the reaction with  $O_2^-$ , being kept at low concentrations and locally limited. But if  $O_2^-$  is quickly removed locally, NO concentrations may be enhanced at greater distances from the thrombus source.

## **4.2 Experimental Evaluations**

The mathematical model shows an elevated level of serotonin close to the collagen surface (12  $\mu\text{M}$  after 1 second), but the electrochemical measurements in the presence of collagen revealed only an average concentration level of 14 nM. This value is several orders of magnitude lower than the mathematical model shows. The sensor had an effective height of 1 mm; therefore, all measurements made are space averaged over the sensor's surface area. The concentration profile of the model indicates a maximum concentration level within the first 10 microns, which sharply attenuates between 10 and 100 microns. Therefore, a low-level serotonin concentration was expected at the effective distance of the sensing element. When the experiment was performed in the presence of L-NMMA (experiment 4), an elevated level of serotonin could not be detected statistically as hypothesized. This result is not interpreted as no effect from NO, but if an effect was present it was not detectable with the carbon fiber sensors designed for this research.

Microscopic inspection of the platelet aggregates adhered to collagen show a non-uniform aggregation of platelets. The mathematical model assumes uniform adherence in monolayer fashion, with every square area releasing serotonin initially. From the model, it can be concluded that serotonin concentrations are locally elevated at the origin of the aggregate. Due to the diffuse nature of the aggregates *in vitro*, serotonin concentration must be a function of sensor placement location on the surface area. It has been discussed above that the height above the dish is also a factor. Stronger serotonin concentrations may be observed if the probe were placed directly on the surface of a platelet aggregate. In the experiments performed, the probe was randomly positioned and

lowered onto the dish. Perhaps under microscopic observance, particular platelet aggregates could be targeted for probe placement. Results from the electrochemical measurements and microscopy showed similar conclusions. In this context, it appears that NO is not limiting or hindering thrombus formation *in vitro*. It has been extensively reported in the literature that basal levels of NO are continuously released from platelets with elevated levels directly related to activation, adhesion, and aggregation<sup>5,35,60,61</sup>. There are some possibilities of why, NO did not produce a statistically measurable effect in the study.

It is possible the inhibitory function of platelet-derived NO is synergetic with prostacyclin (PGI<sub>2</sub>), a compound produced from arachidonate metabolism in the endothelial and smooth muscle cells of blood vessels<sup>34</sup>. PGI<sub>2</sub> is a potent vasodilator and inhibitor of platelet aggregation. Figure 34 illustrates the mechanism of platelet inhibition by PGI<sub>2</sub>. Platelet membranes contain a receptor for PGI<sub>2</sub> coupled to adenylate

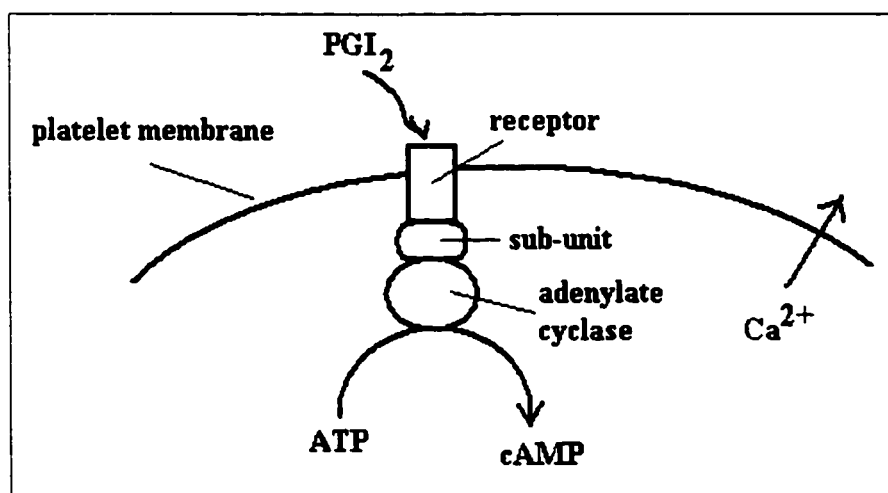


**Figure 34 – Platelet inhibition by PGI<sub>2</sub>**

cyclase through a stimulatory subunit. When PGI<sub>2</sub> reacts with its receptor, on the platelet membrane, adenylate cyclase is activated and rapidly converts intracellular adenosine

triphosphate (ATP) to cyclic adenosine monophosphate (cAMP) <sup>53</sup>. A rise in intraplatelet cAMP concentration causes a cytosolic  $\text{Ca}^{2+}$  shift to a membrane-bound form, resulting in a decrease in free cytosolic  $\text{Ca}^{2+}$  concentration <sup>53</sup>. This mechanism is similar to platelet inhibition by NO. For NO inhibition of platelet function, cumulative evidence suggests that the major mechanism is through activation of platelet soluble guanylate cyclase to increase levels of cGMP <sup>35</sup>. Although both are similar in function, the effect of  $\text{PGI}_2$  is more pronounced due to its longer half-life than NO.

Interestingly,  $\text{TxA}_2$  is also derived from arachidonate, but it functions as an activator of platelet activity rather than an inhibitor (Figure 35). Once platelet adhesion

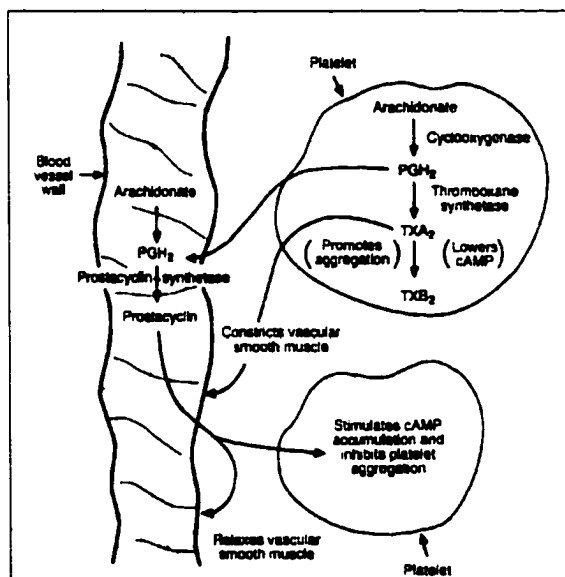


**Figure 35 – Model of  $\text{PGI}_2$  and  $\text{TxA}_2$  production and effects  
(From Gorman, 1979 <sup>62</sup>)**

on the damaged endothelium occurs,  $\text{PGI}_2$  is synthesized to inhibit further aggregation. The combined effect between  $\text{PGI}_2$  and NO might produce critical inhibitor concentrations locally, which are required for platelet inhibition. If the idea of synergism between  $\text{PGI}_2$  and NO is correct, then the absence of one could potentially lead to a

minimal effect with respect to platelet inhibition. The experiments performed in this dissertation were controlled to only contain platelets in diluted PRP. Therefore, PGI<sub>2</sub> was not present in the study, and NO was assumed to be the main inhibitory agent available.

Another possibility of no measurable effect could be attributed to the static dish containing dilute plasma. Under static conditions, the same population of platelets is exposed to the collagen surface for the duration of the experiment. *In vivo*, blood flow through the vasculature continuously circulates the entire platelet population over time. If a vessel injury were present, thus initiating platelet activation and adhesion, fresh platelets would be exposed to the injury site continuously until the wound heals. Continuous transport of platelets to the injury could result in a high platelet density with increased surface concentrations of platelet-derived agonists and inhibitors. In a convective flow situation, the axial velocity component appears to be the dominant role of species transport. This assumption is true at distances far from the vessel wall, but it has been shown that large concentration gradients exist at the vessel wall due to decreased velocities as a result of the parabolic velocity profile<sup>48,63</sup>. Platelet aggregates in convective studies have been reported to have elliptical bases with the major axis parallel to the direction of flow<sup>59</sup>. It is assumed in a convective flow situation, there could be an increased surface concentration of platelet agonists and inhibitors allowing a measurable effect of NO function.

### **4.3 Serotonin Measurements and Data Analysis**

In application of the serotonin sensor to blood components, many experimental difficulties had to be overcome. Difficulties include sensitivity, noise, tip fouling, and interfering species. From incremental laboratory measurements, detection limits for the

sensor on average were 4 to 300 nM. This range is in good agreement with serotonin levels found physiologically, which have been published to be between 5.7 and 178 nM<sup>64</sup>. However, the sensitivity of the probe is a function of the instrumentation used to amplify and condition the signal. From baseline recordings in PBS without any electrochemically active species, it was shown that the potentiostat had random fluctuations of 100 pA magnitude. Discrete fluctuations such as these are attributed to machine noise as well as quantization error from the digital to analog conversion process. However, probe sensitivity, with current instrumentation, was found to be approximately 4 nM. This response was represented by a 100 pA deflection from the baseline recording. For the *in vitro* studies performed, measured values of serotonin were at or moderately above baseline indicating that we were close to the noise region of the sensor. A Faraday cage was used to see if the noise source was environmental, but no change in sensitivity or noise level was observed when implemented, therefore indicating possible noise within the sensor (resistor noise). The final sensor developed proved worthy of measuring low levels of serotonin (4 to 300 nM) with a sensitivity of 4 nM.

Another major problem associated with *in vitro* measurements was tip fouling. It is believed that tip fouling occurs due to electrostatic attraction between the positive potential of the working electrode and the negatively charged peptides in plasma<sup>65</sup>. An approach to guard against tip fouling is to coat the carbon fiber surface with Nafion, a perfluorosulfonated derivative of Teflon that acts as an ion-exchange polymer whose films are highly permeable to cations but almost impermeable to anions<sup>66</sup>. When this was applied to the sensor during calibration processes, sensitivity to serotonin was attenuated from 4 nM to approximately 10 nM. Since Nafion is a coating, it creates a

diffusion barrier on the sensing element; therefore, as coating thickness increases, sensitivity decreases. Drs. Jones and Patton from Louisiana Tech University have indicated that serotonin might be slightly negative when dissolved in solution at physiological pH. Therefore, Nafion coating due to electrostatic interaction might retard serotonin transport to the carbon surface resulting in signal attenuation. Therefore, other steps were taken to decrease tip fouling.

Since the experiments were concerned only with blood platelets at physiological concentrations, it was desired to extract different blood components to isolate the source of fouling. It is known that peptides interfere, but the researcher was unsure about formed elements such as erythrocytes. PRP and PPP were tested separately, and the same degree of tip fouling was observed. It was seen in the literature that concentrated platelet suspensions are used for platelet function studies<sup>67-69</sup>. Acting upon this insight we generated PRP, with standard protocols, and then re-suspended the PRP back to the original blood volume. On average 100 mL of blood returned 10 mL of PRP, therefore the interfering peptide and protein contents were diluted by 90% and normal platelet density was achieved. When tests were performed on dilute PRP, there was a strong interference due to uric acid at almost the same potential as serotonin. Addition of uricase enzyme completely eliminated the interference, and subsequent serotonin calibrations were performed with similar results as obtained in PBS.

Concerning the processing of DPV data in Labview, an interpolating polynomial was needed to model the deflection of the oxidation current. Due to the noise in the signal, error would be introduced into the analysis if the minimum value of the peak was chosen as opposed to the minimum of the interpolating function. Since signal

noise was assumed to be a random fluctuation, then the interpolating polynomial would return an average value of the signal at the point of interest. It was found that signals representing low concentrations had good agreement with a 3<sup>rd</sup>-order polynomial, due to its slight parabolic profile. However, as the concentration level increased, a 4<sup>th</sup>-order polynomial was needed for good agreement. This assumption did not represent a problem because the shape of the signal was approximately 4<sup>th</sup>-order. It is not advised to increase the polynomial order, because of large-scale oscillations in the resulting interpolation. As the order of an interpolating function increases, large oscillations occur at sharp discontinuities in the data <sup>70</sup>.

#### **4.4 Concluding Remarks**

In mammalian physiology, NO plays a role in the regulation of vascular tone, hemostasis, neuronal transmission, and cytoskeleton <sup>60</sup>. Platelets secrete a batch of agents that promote coagulation, however they also produce NO, which has the opposite effect of other platelet-derived compounds. With respect to platelet function, it is well documented that platelet-derived NO is partially involved in maintenance of vascular tone and platelet inhibition. From the research conducted in this project, many questions have been postulated concerning the primary role of NO in platelet function.

Since we did not detect a measurable difference in serotonin concentration due to NOS inhibition, it does not mean that platelet function, primarily dense granule release, is unaffected by platelet-derived NO *in vivo*. It is possible that the role of platelet generated NO is enhanced by the possible synergism with PGI<sub>2</sub> or endothelial-derived NO. Inhibitory agents such as NO and PGI<sub>2</sub> are synthesized and released into the circulation through diffusive flux across a phospholipid membrane. Flux is defined as the product of

mass flow rate and surface area. Due to size differences between the platelet and endothelium, the endothelium possesses more effective surface area than the platelets, and hence more NO and PGI<sub>2</sub> are released into the blood stream. This observance may support the idea that the inhibitory role of platelet NO is achieved through synergism with endothelial derived PGI<sub>2</sub> and NO.

In the past few years, it has been suggested that a primary role of platelets within mammalian circulation is in the defense of the host against invading foreign organisms. Perhaps, in this situation, platelet-derived NO's major function is in the role of cyto-stasis in wound healing. Under *in vivo* conditions, open wounds, such as breaks or tears in the endothelium, are subject to bacterial infection. Hemostasis is initiated through platelet transport to the site of injury where activation, adhesion, and aggregation take place. As the platelet-dense thrombus begins to grow, aggregated platelets are synthesizing NO. From the mathematical transport model dealing with NO, surface concentrations can surpass 5 nM. This model assumes a uniform monolayer of adhered platelets. *In vivo*, it is known that platelets adhere to each other in all directions during thrombus growth. It might be possible for local NO concentration directly above the injury to be even higher than on the surface of the thrombus, thus providing the injury with the NO required to inhibit bacterial invasion.

## **4.5 Recommendations for Future Research**

The completion of this dissertation presented a number of different questions that need to be researched in order to determine the exact physiological role of platelet-derived NO. Questions presented were as follows:

1. Does PGI<sub>2</sub> have a synergistic role with platelet-derived NO for inhibition of platelet function?
2. What effect does convection have on platelet deposition and dense granule release?
3. Through micro-manufacturing techniques, can the serotonin sensor be fabricated to resolve sub-nanomolar concentrations with a high degree of sensitivity?
4. Can a sensor be fabricated to circumvent fouling and uric acid interference?

To resolve the effects of PGI<sub>2</sub>, a similar experiment can be performed using some of the methods used in this project. Since PGI<sub>2</sub> is exclusively made in the vessel wall, performing a study with dilute PRP as in this project can control it<sup>62</sup>. The following combinations would be tested with collagen again as the platelet activator and serotonin would again be measured: (1) PGI<sub>2</sub> in dilute PRP (2) PGI<sub>2</sub> in dilute PRP with L-NMMA (3) dilute PRP and (4) dilute PRP with L-NMMA. By performing this study, information would be gained about the combined effects of PGI<sub>2</sub> and platelet NO.

Two types on convective studies can be performed. Initially, the collagen-coated dish could be gently mixed using an orbital oscillator. The orbital motion would cause the dilute PRP to gently mix in the dish and thereby increase the convective transport of more platelets to the collagen surface for potential activation. If platelet inhibition by NO

is a function of convective transport, an increase in serotonin concentration should result with addition of L-NMMA.

The second type of convective study would involve an *in vitro* flow simulation. The flow simulation would consist of a silicon model with a straight-tube geometry coated in the center with a segment of collagen. A stepper motor driven syringe pump would be used to force diluted PRP, with and without L-NMMA, through the model at a constant Reynolds number. Incorporated within the model, a serotonin sensor would be placed directly next to the collagen surface. Figure 36 illustrates the proposed flow model. Following the flow simulation, histological analysis on the collagen surface would be performed as a means to support the DPV data.

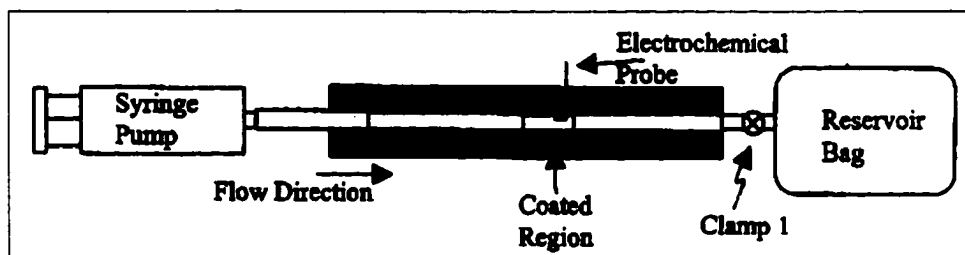


**Figure 36 – *In vitro* flow simulation apparatus**

Through the use of micro manufacturing technology, it might be possible to create a carbon fiber-based electrode system with sub-micron surface area, high sensitivity, and extensive linear range. It is believed that greater sensitivity could be achieved if an amplification system were connected directly to the sensing element. In the current system used for signal conditioning and amplification, the three-electrode system is connected to the potentiostat through a five-foot length cable. Since the electrode is recording values on the order of nanoamps, noise interference might be significant. If the signal was amplified with a gain of only  $10^4$ , line loss and signal resolution would be

increased. Sensitivity to sub-nanomolar levels would further assist in determining the primary function of platelet-derived nitric oxide.

**APPENDIX A**  
**AGONSIT AND INHIBITOR GENERATION**  
**MODEL**

## **Description of Model**

A transient mathematical model to simulate the passive diffusion of platelet generated agonists and inhibitors was developed. Upon local activation by collagen (a strong platelet activator), the platelet membrane catalyzes the production of agonists and inhibitors such as TxA<sub>2</sub>, thrombin, and NO.

## **Modeling Assumptions**

1. Diffusion model obeys Fick's law
2. Constant densities and diffusion coefficients
3. Transient analysis in cylindrical coordinates (r,θ, z) spaced averaged in r and θ
4. Diffusive transport dominate only in z direction
5. Consumption of species in plasma through 1<sup>st</sup> order reactions rates (k)
6. Constant flux of species occurring at collagen surface (K)
7. Negligible initial plasma concentration of species
8. Species concentration approaches zero at an infinite distance from the surface

## **Mathematical Description**

Application of the shell balance method under the guidelines of the assumptions above, the following equation results:

$$\frac{\partial C_A(t, z)}{\partial t} = D_{AB} \frac{\partial^2 C_A(t, z)}{\partial z^2} - kC_A(t, z)$$

## **Boundary and Initial Conditions**

1. The initial condition is represented by  $C_A(0, z) = 0$ , which implies the concentration of species A for all of length z is negligible for time less than or equal to zero.
2. Boundary condition # 1 is represented by  $C(t, \infty) = 0$ , which defines the concentration of species A for all time at an infinite distance is negligible.
3. Boundary condition # 2 states the surface flux of species A was modeled as a zero-order heterogeneous reaction (K) as shown below.

$$-D_{AB} \frac{\partial C(t, 0)}{\partial z} = K$$

## **Solution to Governing Equation**

Although the governing equation was homogeneous, the flux boundary condition was heterogeneous. Therefore, the separation of variables method for solving PDE's was not

applicable; therefore, a Laplace transform method was applied. The solution is described in the following steps.

### **Step 1**

Use the Laplace transform to transform the time variable [ $C_A(t) \leftrightarrow F(s)$ ] in the governing equations and boundary conditions. The governing PDE transforms to:

$$-C_A(0, z) + sF(s; z) = D_{AB}F''(s; z) - kF(s; z)$$

After substituting in the initial condition, the resulting ordinary differential equation reduces to:

$$F''(s; z) - \left( \frac{s+k}{D_{AB}} \right) F(s; z) = 0$$

This is subject to the following transformed boundary conditions:

$$F(s; \infty) = 0 \quad \text{and} \quad F'(s; 0) = \frac{K}{sD_{AB}}$$

### **Step 2**

The general solution to the resulting ordinary differential equation is:

$$F(s; y) = Ae^{-z \sqrt{\frac{s+k}{D_{AB}}}} + Be^{z \sqrt{\frac{s+k}{D_{AB}}}}, \quad \text{where } A \text{ and } B \text{ are unknown constants.}$$

### **Step 3**

The constants A and B are now evaluated. When the infinite boundary condition is substituted into the general solution, an infinite value results due to the positive infinite exponent of  $e$ . Since we know that a finite solution exists, B must be equal to zero. Therefore, the general solution is now:

$$F(s; z) = Ae^{-z \sqrt{\frac{s+k}{D_{AB}}}}$$

To incorporate the remaining boundary condition, we must take the derivative of  $F(s; z)$ .

$$F'(s; z) = -A \sqrt{\frac{s+k}{D_{AB}}} e^{-z \sqrt{\frac{s+k}{D_{AB}}}}$$

After evaluation of the surface boundary condition, we find that  $A = -\frac{K}{s\sqrt{D_{AB}}\sqrt{s+k}}$

The particular solution to this problem is

$$F(s; z) = \frac{K}{s\sqrt{D_{AB}}\sqrt{s+k}} e^{-z\sqrt{D_{AB}}\sqrt{s+k}}$$

#### **Step 4**

The definition of the inverse Laplace transform ( $L^{-1}$ ) is applied to transform the solution from  $s$  domain to time ( $t$ ). From inspection of a table of inverse Laplace transforms, an exact inverse transform does not exist, therefore properties of the Laplace transform can be used to arrive at an integral solution. Application of the inverse transform is shown below:

$$C_A(t, z) = \frac{K}{\sqrt{D_{AB}}} L^{-1} \left[ \frac{1}{s} \frac{e^{-z\sqrt{D_{AB}}\sqrt{s+k}}}{\sqrt{s+k}} \right]$$

In the Laplace transform, division by powers of  $s$  is the same as integration in the time domain from 0 to  $t$ . The result of this application is

$$C_A(t, z) = \frac{K}{\sqrt{D_{AB}}} \int_0^t L^{-1} \left[ \frac{e^{-z\sqrt{D_{AB}}\sqrt{s+k}}}{\sqrt{s+k}} \right] du$$

Next, the time shifting property was used:  $L^{-1}[f(s-a)] = e^{at} F(t)$

$$C_A(t, z) = \frac{K}{\sqrt{D_{AB}}} \int_0^t e^{-kt} L^{-1} \left[ \frac{e^{-z\sqrt{D_{AB}}\sqrt{s}}}{\sqrt{s}} \right] du$$

Now, the remaining part to be transformed is found in a standard transform table. The transform identity is shown below:

$$L^{-1} \left[ \frac{e^{a/s}}{\sqrt{s}} \right] \Leftrightarrow \frac{e^{-\frac{a^2}{4t}}}{\sqrt{\pi t}}, \text{ which returns the solution: } C_A(t, z) = \frac{K}{\sqrt{\pi D_{AB}}} \int_0^t \frac{e^{-\left(ku + \frac{z^2}{4D_{AB}u}\right)}}{\sqrt{u}} du$$

**APPENDIX B**  
**AGONIST RELEASE MODEL**

## **Description of Model**

A transient mathematical model to simulate the passive diffusion of agonists released from platelets was developed. Upon local activation by collagen (a strong platelet activator), the released alpha and dense granule contents. Released agonists of interest are serotonin and ADP.

## **Modeling Assumptions**

1. Diffusion model obeys Fick's law
2. Constant densities and diffusion coefficients
3. Transient analysis in cylindrical coordinates  $(r, \theta, z)$  spaced averaged in  $r$  and  $\theta$
4. Diffusive transport dominate only in  $z$  direction
5. No consumption of species
6. Species are immediately released upon activation (No flux)
7. Negligible initial plasma concentration of species
8. Species concentration approaches zero at an infinite distance from the surface

## **Mathematical Description**

Application of the shell balance method under the guidelines of the assumptions above, the following equation results:

$$\frac{\partial C_A(t, z)}{\partial t} = D_{AB} \frac{\partial^2 C_A(t, z)}{\partial z^2}$$

## **Boundary and Initial Conditions**

1. The initial condition is represented by  $C_A(0, z) = \delta(z)m_0$ , which implies the concentration of species A is instantly released at the surface when time is zero.  $m_0$  represents the amount of species released per square area.
2. Boundary condition # 1 is represented by  $C(t, \infty) = 0$ , which defines the concentration of species A for all time at an infinite distance is negligible.
3. Boundary condition # 2 states the no flux condition for all time at the surface

$$-D_{AB} \frac{\partial C(t, 0)}{\partial z} = 0$$

## **Solution to Governing Equation**

Although the governing equation was homogeneous, the flux boundary condition was heterogeneous. Therefore, the separation of variables method for solving PDE's was not

applicable; therefore, a Fourier transform method was applied. The solution is described in the following steps.

### **Step 1**

Use the Fourier transform to transform the space variable [ $C_A(z) \leftrightarrow F(\omega)$ ] in the governing equations and boundary conditions. The governing PDE transforms to

$$F'(t; \omega) = D_{AB} [i\omega]^2 F(t; \omega)$$

After simplifying this relation and rearranging terms, we arrive at

$$F'(t; \omega) + D_{AB} \omega^2 F(t; \omega) = 0$$

This is subject to the following transformed boundary conditions:

$$F(t; \infty) = 0 \text{ and } F(0, \omega) = m_0$$

### **Step 2**

The general solution to the resulting ordinary differential equation is

$$F(t; \omega) = C e^{-D_{AB} \omega^2 t}, \text{ where } C \text{ is an unknown constant.}$$

### **Step 3**

The constant  $C$  is now evaluated through use of the surface boundary condition:

$$C = m_0$$

The particular solution to this problem is

$$F(t; \omega) = m_0 e^{-D_{AB} \omega^2 t}$$

### **Step 4**

The definition of the inverse Fourier transform ( $F^{-1}$ ) is applied to transform the solution from  $\omega$  domain to position ( $z$ ). From inspection of inverse Fourier transform tables, an exact inverse transform was not found, therefore direct implementation of the inverse Fourier transform is required and is shown below.

$$C_A(t, z) = \frac{1}{2\pi} \int_{-\infty}^{\infty} (m_0 e^{-D_{AB} \omega^2 t}) e^{i\omega z} d\omega$$

Simplification of the above expression returns

$$C_A(t, z) = \frac{m_0}{2\pi} e^{-\frac{z^2}{4D_{AB}t}} \int_{-\infty}^{\infty} e^{-\sqrt{D_{AB}t} \left[ \omega^2 - \frac{iz}{2D_{AB}t} \right]} d\omega$$

Evaluation of the integral involves a variable transformation as follows:

$$\text{Let } \eta = \sqrt{D_{AB}t} \left( \omega - \frac{iz}{2D_{AB}t} \right), \text{ then } d\eta = \sqrt{D_{AB}t} d\omega$$

When the new variables are back substituted, the integral has the form

$$\frac{1}{\sqrt{D_{AB}t}} \int_{-\infty}^{\infty} e^{-\eta^2} d\eta, \text{ which simplifies to } \sqrt{\frac{\pi}{D_{AB}t}}$$

Therefore, the solution to the agonist release model is  $C_A(t, z) = \frac{m_0}{2\sqrt{\pi D_{AB}t}} e^{-\frac{z^2}{4D_{AB}t}}$

## LIST OF WORKS CITED

1. Prentice, C.R. Pathogenesis of thrombosis. *Haemostasis* **20 Suppl 1**, 50-9 (1990).
2. Fuster, V. Lewis A. Conner Memorial Lecture. Mechanisms leading to myocardial infarction: insights from studies of vascular biology [published erratum appears in *Circulation* 1995 Jan 1;91(1):256]. *Circulation* **90**, 2126-46 (1994).
3. Sixma, J.J. & de Groot, P.G. von Willebrand factor and the blood vessel wall. *Mayo Clinic Proceedings* **66**, 628-33 (1991).
4. Copley, A.L. Roles of platelets in physiological defense mechanism and pathological conditions. *Folia Haematol.* **106**, 732-764 (1979).
5. Herd, C.M. & Page, C.P. Do platelets have a role as inflammatory cells? in *Immunopharmacology of platelets* (ed. Joseph, M.) (Harcourt Brace and Company, London, 1995).
6. Nachman, R.L. & Weksler, B.B. The platelet as an inflammatory cell. in *The Cell Biology of Inflammation* (ed. Weissmann, G.) 145-162 (Elsevier, Amsterdam, 1980).
7. Falk, E. & Fernández-Ortiz, A. Role of thrombosis in atherosclerosis and its complications. *American Journal Of Cardiology* **75**, 3B-11B (1995).
8. Berliner, J.A. *et al.* Atherosclerosis: basic mechanisms. Oxidation, inflammation, and genetics. *Circulation* **91**, 2488-96 (1995).
9. Schroeder, A.P. & Falk, E. Vulnerable and dangerous coronary plaques. *Atherosclerosis* **118 Suppl**, S141-9 (1995).
10. MacIsaac, A.I., Thomas, J.D. & Topol, E.J. Toward the quiescent coronary plaque. *Journal Of The American College Of Cardiology* **22**, 1228-41 (1993).
11. Ruggeri, Z.M. & Ware, J. von Willebrand factor. *Faseb Journal* **7**, 308-16 (1993).
12. Fuster, V. *et al.* Atherosclerotic plaque rupture and thrombosis. Evolving concepts. *Circulation* **82**, II47-59 (1990).

13. Glagov, S., Zarins, C., Giddens, D.P. & Ku, D.N. Hemodynamics and atherosclerosis. Insights and perspectives gained from studies of human arteries. *Archives Of Pathology And Laboratory Medicine* **112**, 1018-31 (1988).
14. Schroeder, A.P. & Falk, E. Pathophysiology and inflammatory aspects of plaque rupture. *Cardiology Clinics* **14**, 211-20 (1996).
15. Turgeon, M.L. *Clinical Hematology: Theory and Procedures*, 479 (Little, Brown, and Company, Boston, 1993).
16. Harmening, D.M. *Clinical Hematology and Fundamentals of Hemostasis*, (F. A. Davis Company, Philadelphia, 1997).
17. Eisenberg, P.R. Thrombosis and fibrinolysis in acute myocardial infarction. *Alcoholism, Clinical And Experimental Research* **18**, 97-104 (1994).
18. Hellums, J.D. 1993 Whitaker Lecture: biorheology in thrombosis research. *Annals Of Biomedical Engineering* **22**, 445-55 (1994).
19. McKenzie, S.B. *Textbook of Hematology*, (Lea and Febiger, Philadelphia, 1988).
20. Le Breton, H., Plow, E.F. & Topol, E.J. Role of platelets in restenosis after percutaneous coronary revascularization. *Journal Of The American College Of Cardiology* **28**, 1643-51 (1996).
21. Monsen, C.H., Adams, P.C., Badimon, L., Chesebro, J.H. & Fuster, V. Platelet-vessel wall interactions in the development of restenosis after coronary angioplasty. *Zeitschrift Fur Kardiologie* **76 Suppl 6**, 23-8 (1987).
22. Faull, R.J., Du, X. & Ginsberg, M.H. Receptors on platelets. *Methods In Enzymology* **245**, 183-94 (1994).
23. Frojmovic, M.M. Platelet aggregation in flow: differential roles for adhesive receptors and ligands. *American Heart Journal* **135**, S119-31 (1998).
24. Hubbell, J.A. & McIntire, L.V. Platelet active concentration profiles near growing thrombi. A mathematical consideration. *Biophysical Journal* **50**, 937-45 (1986).
25. Adams, G.A. & Feuerstein, I.A. Platelet adhesion and release: interfacial concentration of released materials. *American Journal Of Physiology* **240**, H99-108 (1981).
26. Badimon, L., Chesebro, J.H. & Badimon, J.J. Thrombus formation on ruptured atherosclerotic plaques and rethrombosis on evolving thrombi. *Circulation* **86**, III74-85 (1992).

27. Li, N., Wallen, N.H., Ladjevardi, M. & Hjemdahl, P. Effects of serotonin on platelet activation in whole blood. *Blood Coagulation and Fibrinolysis* **8**, 517-23 (1997).
28. Munter, W.A. & Stein, P.D. Newtonian behavior of blood at high rates of shear. *Biorheology* **10**, 501-8 (1973).
29. Hanson, S.R. & Sakariassen, K.S. Blood flow and antithrombotic drug effects. *American Heart Journal* **135**, S132-45 (1998).
30. Schoephoerster, R.T., Oynes, F., Nunez, G., Kapadvanjwala, M. & Dewanjee, M.K. Effects of local geometry and fluid dynamics on regional platelet deposition on artificial surfaces. *Arteriosclerosis And Thrombosis* **13**, 1806-13 (1993).
31. Aarts, P.A. *et al.* Blood platelets are concentrated near the wall and red blood cells, in the center in flowing blood. *Arteriosclerosis* **8**, 819-24 (1988).
32. Brown, C.H.d., Leverett, L.B., Lewis, C.W., Alfrey, C.P.J. & Hellums, J.D. Morphological, biochemical, and functional changes in human platelets subjected to shear stress. *Journal Of Laboratory And Clinical Medicine* **86**, 462-71 (1975).
33. Loscalzo, J. & Radomski, M.W. Platelet Bioassays of Nitric Oxide and Related Congeners. in *Methods in Nitric Oxide Research* (eds. Feelisch, M. & Stamler, J.S.) 583-591 (John Wiley and Sons Ltd., 1996).
34. Kawai, C. Pathogenesis of acute myocardial infarction. Novel regulatory systems of bioactive substances in the vessel wall. *Circulation* **90**, 1033-43 (1994).
35. Riddell, D.R. & Owen, J.S. Nitric oxide and platelet aggregation. *Vitamins And Hormones* **57**, 25-48 (1999).
36. Knowles, R.G., Ferrige, A.G. & Moncada, S. Nitric oxide release accounts for the biological activity of endothelium-derived relaxing factor. *Nature* **327**, 524-526 (1987).
37. Yang, Z. & Lüscher, T.F. Basic cellular mechanisms of coronary bypass graft disease. *European Heart Journal* **14 Suppl I**, 193-7 (1993).
38. Ramamurthi, A. & Lewis, R.S. Design of a novel apparatus to study nitric oxide (NO) inhibition of platelet adhesion. *Annals Of Biomedical Engineering* **26**, 1036-43 (1998).
39. Beckman, J.S. & Koppenol, W.H. Nitric oxide, superoxide, and peroxynitrite: the good, the bad, and ugly. *american journal of physiology* **271**, C1424-37 (1996).

40. Stamler, J.S., Singel, D.J. & Loscalzo, J. Biochemistry of nitric oxide and its redox-activated forms [see comments]. *science* **258**, 1898-902 (1992).
41. Sorensen, E.N., Burgreen, G.W., Wagner, W.R. & Antaki, J.F. Computational Simulation of Platelet Deposition and Activation: I. Model Development and Properties. *Annals of Biomedical Engineering* **27**, 436-448 (1999).
42. Wagner, W.R. & Hubbell, J.A. Local thrombin synthesis and fibrin formation in an in vitro thrombus model resulting in platelet recruitment and thrombus stabilization on collagen and heparinized blood. *Journal of Laboratory and Clinical Medicine* **116**, 636-650 (1989).
43. Skoog, D.A., Holler, F.J. & Nieman, T.A. Chapter 25: Voltammetry. in *Principles of Instrumental Analysis* 639-671 (Saunders College Publishing, Philadelphia, 1998).
44. Kawagoe, K.T., Zimmerman, J.B. & Wightman, R.M. Principles of voltammetry and microelectrode surface states. *Journal of Neuroscience Methods* **48**, 225-40 (1993).
45. Rice, M.E. & Nicholson, C. Measurement of nonomolar dopamine diffusion using low-noise perfluorinated ionomer coated carbon fiber microelectrodes and high-speed cyclic voltammetry. *Analytical Chemistry* **61**, 1805-1810 (1989).
46. Duda, C.T. & Brunlett, C.S. Amperometric Techniques. in *Handbook of Instrumental Technique for Analytical Chemistry* 691-708 .
47. Adams, G.A. & Feuerstein, I.A. Maximum fluid concentrations of materials released from platelets at a surface. *American Journal Of Physiology* **244**, H109-14 (1983).
48. Bird, R.B., Stewart, W.E. & Lightfoot, E.N. *Transport Phenomena*, 780 (John Wiley and Sons, New York, 1960).
49. Volf, I. *et al.* Stimulating effect of biologically modified low density lipoproteins on ADP-induced aggregation of washed platelets persists in absence of specific binding. *Thrombosis Research* **97**, 441-9 (2000).
50. Gonon, F.G., Buda, M., Cespuaglio, R., Jouvet, M. & Pujol, J.F. In vivo electrochemical detection of catechols in the neostriatum of anesthetized rats: dopamine or DOPAC? *Nature* **286**, 902-904 (1980).
51. Gonon, F., Buda, M. & Pujol, J.F. Treated carbon fibre electrodes for measuring catechols and ascorbic acid. in *Measurement of Neurotransmitter Release In Vivo* (ed. Marsden, C.A.) 153-171 (Wiley, New York, 1984).

52. Lantoine, F., Trevin, S., Bedioui, F. & Devynck, J. Selective and sensitive electrochemical measurement of nitric oxide in aqueous solution: discussion and results. *Journal of Electroanalytical Chemistry* **392**, 85-89 (1995).
53. Corriveau, D.M. & Fritsma, D.A. *Hemostasis and Thrombosis in the Clinical Laboratory*, 443 (J. B. Lippincott Company, Philadelphia, 1988).
54. Sheehan, D.C. & Hrapchak, B.B. Acridine orange fluorescent method for DNA and RNA. in *Theory and practice of histotechnology* 152-153 (The C. V. Mosby Company, St. Louis, 1980).
55. Mahony, C. & Ferguson, J. The effect of heparin versus citrate on blood echogenicity in vitro: the role of platelet and platelet-neutrophil aggregates. *Ultrasound In Medicine And Biology* **18**, 851-9 (1992).
56. Bull, D.R. *et al.* Application of fast cyclic voltammetry to measurement of electrically evoked DA overflow from brain slices in vitro. *J. Neurosci. Methods* **32**, 37-44 (1990).
57. Cespuglio, R., Sarda, N., Gharib, A., Faradji, H. & Chastrette, N. Differential pulse voltammetry in vivo with working carbon fiber electrodes: 5-hydroxyindole compounds or uric acid detection? *Experimental Brain Research* **64**, 589-95 (1986).
58. Montgomery, D.C. *Design and Analysis of Experiments*, 704 (John Wiley and Sons, New York, 1996).
59. Adams, G.A., Brown, S.J., McIntire, L.V., Eskin, S.G. & Martin, R.R. Kinetics of platelet adhesion and thrombus growth. *Blood* **62**, 69-74 (1983).
60. Zhou, Q., Hellermann, G.R. & Solomonson, L.P. Nitric oxide release from resting human platelets. *Thrombosis Research* **77**, 87-96 (1995).
61. Goulielmos, N.V., Enayat, Z.E., Sheridan, D.J., Cohen, H. & Flores, N.A. Nitric oxide and prostacyclin modulate the alterations in cardiac action potential duration mediated by platelets during ischaemia. *Cardiovascular Research* **30**, 788-98 (1995).
62. Gorman, R. Modulation of human platelet function by prostacyclin and thromboxane A<sub>2</sub>. *Federation Proceedings* **38**, 83-88 (1979).
63. Stubley, G.D., Strong, A.B., Hale, W.E. & Absolom, D.R. A review of mathematical models for the prediction of blood cell adhesion. *PCH PhysicoChemical Hydrodynamics* **8**, 221-235 (1987).

64. Diem, K. & Lentner, C. (eds.). *Geigy Scientific Tables*, (Ciba-Geigy Limited, Swit., 1970).
65. Netchiporouk, L.I., Shram, N.F., Jaffrezic\_Renault, N., Martelet, C. & Cespuglio, R. In vivo brain glucose measurements: differential normal pulse voltammetry with enzyme-modified carbon fiber microelectrodes. *Analytical Chemistry* **68**, 4358-64 (1996).
66. Gerhardt, G.A., Oke, A.F., Nagy, G., Moghaddam, B. & Adams, R.N. Nafion-coated electrodes with high selectivity for CNS electrochemistry. *Brain Research* **290**, 390-5 (1984).
67. Bowry, S.K. & Muller\_Berghaus, G. Preparation of washed platelets from non-anticoagulated human blood. *Thrombosis Research* **43**, 621-33 (1986).
68. Pineda, A.A., Zylstra, V.W., Clare, D.E., Dewanjee, M.K. & Forstrom, L.A. Viability and functional integrity of washed platelets. *Transfusion* **29**, 524-7 (1989).
69. Shukla, S.D., Morrison, W.J. & Klachko, D.M. Response to platelet-activating factor in human platelets stored and aged in plasma. Decrease in aggregation, phosphoinositide turnover, and receptor affinity. *Transfusion* **29**, 528-33 .
70. Burden, R.L. & Faires, J.D. *Numerical Analysis*, 811 (Brooks/Cole Publishing Company, Pacific Grove, CA, 1997).